LUND UNIVERSITY

Novel Diagnostic Tools for Skin and Periorbital Cancer - Exploring Photoacoustic Imaging and Diffuse Reflectance Spectroscopy

Dahlstrand, Ulf

2020

Novel Diagnostic Tools for Skin and Periorbital Cancer

Exploring Photoacoustic Imaging and Diffuse Reflectance Spectroscopy

ULF DAHLSTRAND | DEPARTMENT OF CLINICAL SCIENCES, LUND | LUND UNIVERSITY

Ulf Dahlstrand received his medical degree from Lund University in 2009. He is an ophthalmologist specialized in oculoplastic and strabismus surgery. This thesis explores novel non-invasive techniques for diagnosing and delineating skin and eyelid tumors.

Ulf is a common name in Scandinavia and is derived from *úlfr*, the Old Norse word for 'wolf'.

FACULTY OF MEDICINE

LUND UNIVERSITY

Novel Diagnostic Tools for Skin and Periorbital Cancer

Novel Diagnostic Tools for Skin and Periorbital Cancer

Exploring Photoacoustic Imaging and Diffuse Reflectance Spectroscopy

Ulf Dahlstrand, MD

LUND
UNIVERSITY

DOCTORAL DISSERTATION
by due permission of the Faculty of Medicine, Lund University, Sweden.
To be defended at 13.00 the 20th of March 2020, in Segerfalksalen at BMC, Lund.

Faculty opponent
Marcelo Ayala, MD, PhD
Associate professor, Sahlgrenska Academy, University of Gothenburg

Organization LUND UNIVERSITY Faculty of Medicine Department of Clinical Sciences Lund Ophthalmology, Lund, Sweden	Document name DOCTORAL DISSERTATION
	Date of issue: 2020-03-20
Author(s): Ulf Dahlstrand	Sponsoring organization

Title and subtitle
Novel Diagnostic Tools for Skin and Periorbital Cancer. Exploring Photoacoustic Imaging and Diffuse Reflectance Spectroscopy

Abstract

The eyelids are susceptible to a number of skin cancers which are challenging to excise radically without sacrificing excessive healthy tissue. The way in which a tumor is delineated preoperatively has not changed significantly over the past century. The aims of the work presented in this thesis were to investigate two novel non-invasive techniques for diagnosing and delineating skin tumors.

Extended-wavelength diffuse reflectance spectroscopy (EWDRS) was evaluated to determine its ability to differentiate between and classify different skin and tissue types in an *in vivo* pig model, with the aid of machine learning methods. The recordings were used to train a support vector machine, and it was possible to perform classifications with an overall accuracy of over 98%. The ability of EWDRS to identify the borders of pigmented skin lesions in an *in vivo* pig model was also evaluated. Using a thin probe, it was possible to detect the border with a median discrepancy of 70 μm, compared to the border found on histological examination.

Photoacoustic imaging (PAI), a biomedical imaging modality that combines laser irradiation and ultrasound, was used to examine basal cell carcinomas (BCCs) and human eyelids *ex vivo*. Typical photoacoustic spectra were observed for BCCs as well as for the different layers of the healthy eyelid, and these structures could be visualized in three-dimensional images. A case was described in which PAI showed that the pentagonal excision of an eyelid BCC was non-radical, as was later confirmed by histological examination.

In conclusion, both EWDRS and PAI are capable of differentiating between different kinds of tissue and, following further development and studies, could potentially be used to diagnose and delineate skin and eyelid tumors prior to surgical excision.

Key words: Skin cancer, periorbital, eyelid, oculoplastic, diffuse reflectance spectroscopy, photoacoustic imaging

Classification system and/or index terms (if any)

Supplementary bibliographical information	Language: English
ISSN: 1652-8220	ISBN: 978-91-7619-891-9

Recipient's notes	Number of pages: 67	Price
	Security classification	

Novel Diagnostic Tools for Skin and Periorbital Cancer

Exploring Photoacoustic Imaging and Diffuse Reflectance Spectroscopy

Ulf Dahlstrand, MD

LUND
UNIVERSITY

To Viviénne, Vincent, Wilhelm and Eveline

The more you know, the more you know you don't know.

– Aristoteles (384 – 322 BC)

Det kan väl inte vara så svårt att hitta på ett eget citat?

– Ulf Dahlstrand (AD 1981 -)

Contents

Abstract

The eyelids are susceptible to a number of skin cancers which are challenging to excise radically without sacrificing excessive healthy tissue. The way in which a tumor is delineated preoperatively has not changed significantly over the past century. The aims of the work presented in this thesis were to investigate two novel non-invasive techniques for diagnosing and delineating skin tumors.

Extended-wavelength diffuse reflectance spectroscopy (EWDRS) was evaluated to determine its ability to differentiate between and classify different skin and tissue types in an *in vivo* pig model, with the aid of machine learning methods. The recordings were used to train a support vector machine, and it was possible to perform classifications with an overall accuracy of over 98%. The ability of EWDRS to identify the borders of pigmented skin lesions in an *in vivo* pig model was also evaluated. Using a thin probe, it was possible to detect the border with a median discrepancy of 70 μm, compared to the border found on histological examination.

Photoacoustic imaging (PAI), a biomedical imaging modality that combines laser irradiation and ultrasound, was used to examine basal cell carcinomas (BCCs) and human eyelids *ex vivo*. Typical photoacoustic spectra were observed for BCCs as well as for the different layers of the healthy eyelid, and these structures could be visualized in three-dimensional images. A case was described in which PAI showed that the pentagonal excision of an eyelid BCC was non-radical, as was later confirmed by histological examination.

In conclusion, both EWDRS and PAI are capable of differentiating between different kinds of tissue and, following further development and studies, could potentially be used to diagnose and delineate skin and eyelid tumors prior to surgical excision.

Papers included in this thesis

This thesis is based on the following five papers, which will be referred to in the text by their Roman numerals. The papers are reproduced with the permission of the respective publisher.

I.   **Dahlstrand U**, Sheikh R, Nguyen CD, Memarzadeh K, Reistad N, Malmsjo M: Extended-wavelength diffuse reflectance spectroscopy with a machine-learning method for *in vivo* tissue classification. *PLoS One*. 2019 Oct 10;14(10):e0223682.

II. **Dahlstrand U**, Sheikh R, Nguyen CD, Hult J, Reistad N, Malmsjo M: Identification of tumor margins using diffuse reflectance spectroscopy with an extended-wavelength spectrum in a porcine model. *Skin Res Technol.* 2018;24(4):667-671.

III. **Dahlstrand U**, Sheikh R, Merdasa, A, Chakari R, Persson B, Cinthio M, Erlov T, Gesslein B, Malmsjo M: Photoacoustic imaging for three-dimensional visualization and delineation of basal cell carcinoma in patients. Submitted 2019.

IV. **Dahlstrand U**, Sheikh R, Berggren J, Hult J, Albinsson J, Cinthio M, Malmsjo M: Spectral Signatures in the Different Layers of the Human Eyelid by Photoacoustic Imaging. *Lasers Surg Med.* 2019 Aug 22. doi: 10.1002/lsm.23148. [Epub ahead of print]

V.   ***Dahlstrand U**, Sheikh R, Malmsjo M: Photoacoustic imaging for intraoperative micrographic control of the surgical margins of eyelid tumours. *Acta Ophthalmol.* 2019 Sep 6. doi: 10.1111/aos.14245. [Epub ahead of print]

*Study V is a case report/letter to the editor, and not an original publication.

Abbreviations

BCC	Basal cell carcinoma
DRS	Diffuse reflectance spectroscopy
EWDRS	Extended-wavelength diffuse reflectance spectroscopy
MM	Malignant melanoma
NIR	Near-infrared
NMSC	Non-melanoma skin cancer
PA	Photoacoustic
PAI	Photoacoustic imaging
PCA	Principal component analysis
ROI	Region of interest
SCC	Squamous cell carcinoma
SVM	Support vector machine
SWIR	Short-wave infrared
UV	Ultraviolet
VIS	Visible

Introduction

The primary form of treatment for most skin cancers is surgical excision [1]. Only after surgery, through microscopic examination of the excised tissue, can it be determined whether the tumor has been completely removed, or if additional surgery is needed. In the case of eyelid skin cancer, this information is vital, as reconstructive surgery is often complex, and should ideally not be undertaken before complete excision has been confirmed. Although there has been considerable technological development within the medical field in general, and in diagnostic imaging in particular during the 20th and 21st centuries, little has changed in the clinical approach to skin cancer removal.

The aim of the work described in this thesis was to explore two new techniques, extended-wavelength diffuse reflectance spectroscopy (EWDRS) and photo-acoustic imaging (PAI), which it is hoped will change the way in which skin and eyelid tumors are diagnosed and delineated in the future.

Skin tumors

The normal skin

The skin is one of the largest organs in the human body [2], and is composed of several layers. It acts as the first line of defense against the outer world, and plays an important role in heat regulation, sensation, and the synthesis of vitamin D [3]. The outer layer is called the epidermis, and is composed of four sublayers that represent different stages of maturation of keratinocytes, the main type of cell in the skin. In the most superficial layer, the stratum corneum, the cells are flattened and have lost their nuclei. They are arranged in multiple thin layers and provide an important part of the barrier function. The inner layer of the epidermis, the stratum basale, is where melanocytes are found. Melanocytes are responsible for the production of melanin, the dark pigment that gives the skin its color and protects the tissue from ultraviolet (UV) radiation [4].

Underneath the epidermis is the dermis, which is composed of fibroblasts and dense connective tissue that provide support and nutrients to the epidermis. It contains several of the important structures in the skin, such as the hair follicles,

sweat glands, nerves, lymphatic vessels, and blood vessels. The thickness of the dermis varies with location on the body, but is mostly between 0.6 and 3 mm, in contrast to the epidermis, which is about 0.07 to 0.12 mm thick. Underneath the dermis is the subcutaneous tissue, which varies in thickness from person to person. It contains adipocytes (fat cells), connective tissue, and some larger blood vessels. It contributes to the body's temperature regulation and the ability to absorb mechanical shock, and acts as an energy reserve [4].

Due to its vulnerable location, the skin is susceptible to a large number of pathologies, cancer being one of them. The main cause of skin cancer is UV radiation resulting from exposure to the sun, and the incidence of skin cancer is increasing worldwide [5]. Skin cancer is commonly divided into two main categories, malignant melanoma (MM) and non-melanoma skin cancer (NMSC); the latter including basal cell carcinoma (BCC) and squamous cell carcinoma (SCC) as the dominant components.

Malignant melanoma

Malignant melanomas only account for a few percent of all skin cancers, but constitute a very important group due to the associated high rate of mortality [5]. It is caused mainly by exposure to sunlight, and multiple events of severe sunburn increase the risk further [6]. The epidermal melanocytes are responsible for this form of cancer, and it is clinically usually seen as a dark irregularly pigmented lesion on the skin. Such lesions can arise from an existing benign nevus (mole), but can also emerge *de novo*. One of the most important prognostic factors is the thickness of the tumor at the time of diagnosis. A 4-mm-thick tumor is associated with a substantially higher risk of death within 5 years, than a tumor that is less than 1 mm thick. Deaths due to MM are generally caused by spread through metastases [7].

Non-melanoma skin cancer

Non-melanoma skin cancer is the term used to describe all other kinds of skin cancer apart from MM. It includes BCC, SCC, and more rare forms of skin cancer, such as angiosarcomas and Merkel cell carcinoma. The main focus of the work described in this thesis was on BCC.

Basal cell carcinoma

Basal cell carcinoma is the dominant form among NMSCs, but it is difficult to estimate the exact proportion [8]. It is caused by the abnormal, uncontrolled growth of the basal cells. BCC usually presents as a small papular lesion that enlarges slowly over several months or even years. The appearance differs

depending on the subtype. Many classifications exist, but BCCs are often divided into superficial, nodular, and morpheiform subtypes [9]. Nodular BCC is an elevated pearl-like nodule with telangiectasias on the surface, while superficial BCC grows as a thin erythematous plaque (Figure 1). These are often considered less aggressive, but there are also more infiltrative forms. Morpheiform BCC grows like an infiltrating plaque without clear borders, and can be difficult to distinguish from scars. BCCs are almost always a non-metastatic form of malignancy, but if left untreated the tumors can invade locally, causing significant destruction to the surrounding soft tissues [10].

Figure 1. A superficial BCC on the back of a patient.

Treatment

The first line therapeutic treatment for skin cancer is surgery. The aim is to completely remove the tumor, so that no tumor cells remain in the tissue, in order to avoid recurrence. Traditionally, the border of the tumor is identified by visual inspection by the surgeon, sometimes aided by the use of dermoscopy [1]. An additional, predetermined, margin is then added, and the area is marked out for excision. Melanomas are usually excised with an additional margin of 10 or 20 mm, depending on the thickness of the tumor [11]. BCCs are excised with margins of 3-10 mm beyond the visible tumor border, depending on the size, location, and local clinical practice [12]. After excision, the lesion is sent for histopathological analysis, to confirm the diagnosis, and the margins are inspected to ensure that all the tumor cells have been removed. If tumor cells are found at the edge of the excision, further surgery is necessary. The rate of incomplete excision has been

reported to be between 7 and 25% in the literature for BCCs, making it a significant problem [13]. Non-surgical treatment, such as cryotherapy, photodynamic therapy, radiotherapy, and topical creams, may be suitable in specific cases.

Mohs surgery

An alternative technique for the removal of BCC is Mohs micrographic surgery, which allows examination of the tumor margins through staged resection and simultaneous histopathological examination [14]. The procedure is usually performed under local anesthesia, and the tumor is excised with a small margin. The lesion is then immediately processed, and thin slices of the peripheral and deep margins are cut and examined by a pathologist or dermatosurgeon. If cancer cells are found in any of the sections, their location is communicated to the surgeon, who removes more tissue from that area. This procedure is repeated until no further cancer cells are found, and the wound can then be reconstructed, all in one surgical session [14].

Mohs surgery is considered the most efficient method for the complete removal of high-risk and complicated BCCs, and provides precise removal of the tumor while sparing healthy tissue. For this reason, it is often used in areas where tissue preservation is of the utmost importance, for example, the face, hands, and genitals. However, the procedure is time-consuming and expensive, and depends on the experience of the physician [15-17].

Eyelid tumors

The normal eyelid

The eyelids contain several anatomical structures that keep the eye lubricated and protect it from the outer world. The tarsal plates of the upper and lower eyelids are stiff collagen-dense structures that provide stability, and are anchored to the orbital rim by the medial and lateral canthal ligaments. The orbicularis oculi muscle runs partially over the tarsal plates and plays an important role in lid closure, as well as in the function of the lacrimal pump, ensuring adequate drainage of tears. There is no subcutaneous fat in this region, so the orbicularis muscle is covered by only a thin layer of skin. The inside of the eyelid is lined with the conjunctiva, a thin mucous membrane, that plays a role in protecting the surface of the eye [18].

Eyelid skin tumors

As with the rest of the face, the eyelids are often exposed to the sun, and are thus susceptible to skin cancer. Between 5 and 10 % of all cutaneous tumors occur periorbitally, of which at least 80% are BCCs. They often affect the lower eyelid (Figure 2), but can also be found on the upper eyelid. Melanomas are rare in the periorbital region, accounting for only approximately 1% of malignancies. Other malignancies of the eyelids are SCC, accounting for 5-10% of the tumors in this region, sebaceous carcinomas (1-5%) and Merkel cell carcinomas (very rare) [19].
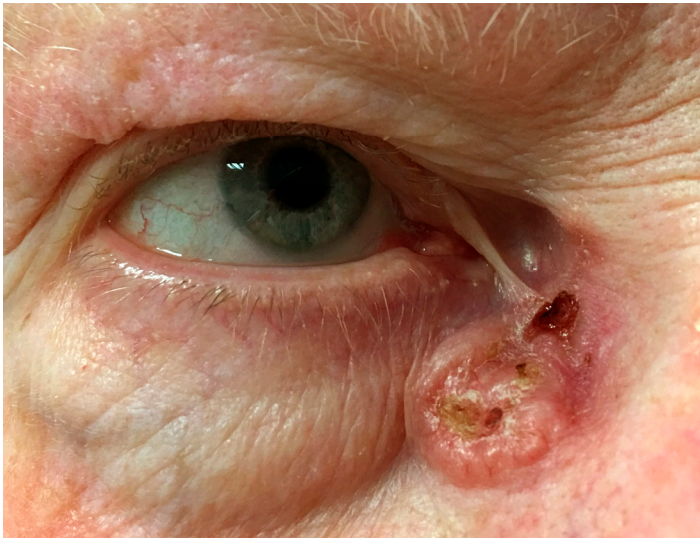
Figure 2. A periorbital nodular BCC in close proximity to the lower eyelid.

Challenges associated with eyelid cancer surgery

The same principles as those used for treatment of skin cancer on the rest of the body also apply to the eyelids, i.e., surgery is the primary option. The lesion is visually assessed by the surgeon and a few millimeters of supposedly healthy tissue are added, before excision and subsequent histopathological analysis. The main difference between the eyelids and the rest of the body lies in the reconstructive phase. The eyelids are vital in protecting the eye, and any defect must be reconstructed so as to maintain the function of the eyelids.

The most common approach in removing a suspected BCC from an eyelid is a full-thickness pentagonal excision (Figure 3). If the amount of tissue removed is less than 30% of the total length of the eyelid it is usually possible to perform a direct closure. If the excised area is larger, then some kind of reconstructive flap or transplantation is usually needed to repair the defect. This can be more or less

complex, and does not always produce a satisfactory result from a cosmetic point of view [20]. Thus, every millimeter of the eyelid that can be spared is important, and excision should therefore be as precise as possible.
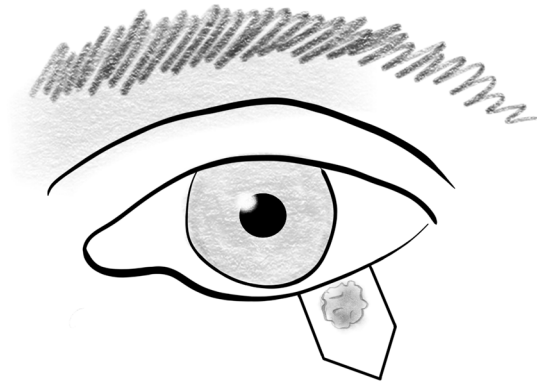
Figure 3. Illustration of the pentagonal excision of a small tumor from the lower eyelid.

Despite the need for precision, the clinical method of preoperative delineation of eyelid tumors has not changed significantly during the past century. In most cases, this relies on visual inspection by the surgeon, without the aid of other tools or techniques.

Existing diagnostic techniques

A number of non-invasive techniques have been investigated, or are being used to provide information on skin lesions prior to surgery; each with advantages and disadvantages.

Dermoscopy

Dermoscopy is carried out with a hand-held device that provides magnification and illumination of the skin, enabling the visualization of microstructures from the epidermis down to the papillary dermis. The information obtained in this way can be used to classify cutaneous cancer [15, 21], and significantly better diagnostic accuracy has been demonstrated with dermoscopy than conventional clinical

examination [22]. However, it is a subjective modality, and requires a trained, experienced user to obtain reliable results [23]. Dermoscopy is commonly used in clinical practice by dermatologists, but is rarely used by ophthalmologists to examine suspected tumors on the eyelids. It could, however, be of some benefit [24].

In vivo reflectance confocal microscopy

Reflectance confocal microscopy is a laser-based method that allows examination down to the depth of the papillary dermis, with a resolution that is close to that of histological analyses. In a meta-analysis, the pooled sensitivity for the diagnosis of several skin cancers has been reported to be 93.2%, while the specificity was only 82.8%. The accuracy of the method also seems to be dependent on the experience of the observer, as the resulting images resemble histological images [25]. Another drawback is that it cannot be used to assess the depth of the tumor. It is rarely used in the periorbital area, but there are a few examples of skilled dermatologists and ophthalmologists working together on eyelid lesions with good results [26] [27].

High-frequency ultrasound

In high-frequency ultrasound, 20 to 100 MHz ultrasound is used to obtain real-time images of the tumor. As most skin tumors are hypoechogenic, its primary use is not in providing a reliable diagnosis, but rather in giving a pre-surgical indication of tumor thickness and its potential infiltrative properties [28]. It was recently concluded in a Cochrane study that insufficient reliable research has been performed to allow any conclusions to be drawn on whether high-frequency ultrasound would be useful in the clinical diagnosis of skin cancers [29].

Optical coherence tomography

Another emerging modality is optical coherence tomography, where reflected light is used to create a cross-sectional view of the skin. The penetration is usually about 1-2 mm, which is deeper than reflectance confocal microscopy, but still not sufficient to image many skin tumors [30]. It can be used to visualize the layered architecture of the skin and some typical features of skin tumors, but with low resolution. The resolution has been improved in recent years, but its added value in diagnosing NMSC is yet to be demonstrated [31]. Some studies have been performed to investigate the use of the technique on eyelid tumors [32] [30].

Diffuse reflectance spectroscopy

Diffuse reflectance spectroscopy (DRS) is a technique that records the reflectance spectrum produced as light interacts with the examined tissue. Illuminating a tissue leads to various degrees of light absorption and the scattering of photons that produce the reflectance spectrum. The shape of this spectrum depends on the wavelengths being used as well as the optical properties and structure of the tissue being examined. A DRS system thus usually contains a well-defined light source and a probe that both delivers the light and collects the diffusely reflected light, as illustrated in Figure 4. The reflected light is analyzed using a spectrometer that displays the intensity of the reflected light as a function of its wavelength [33]. Commonly used spectrometers capture light in the visible to near-infrared range (VIS-NIR; 400 to 1000 nm) or in the near-infrared to short-wave infrared range (NIR-SWIR; 1000 to 1700 nm). A study using light of 455 to 765 nm has shown that it was possible to detect selected MMs and NMSCs with a sensitivity and specificity of about 90% [34].
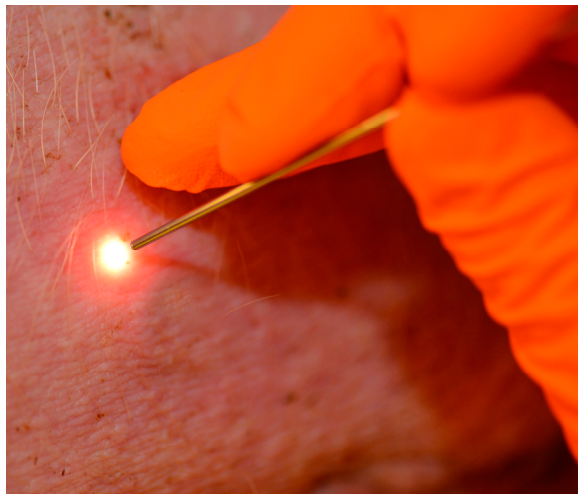
Figure 4. The thin DRS probe used to both deliver the incident light and collect the diffusely reflected light (see Paper II).

The research group at our clinic has recently developed a DRS system that combines two spectrometers (VIS-NIR and NIR-SWIR) to visualize an extended-wavelength spectrum between 450 and 1550 nm [35-37]. Melanin and hemoglobin (both oxygenated and deoxygenated) are the most important chromophores in the skin, and absorb most of the light in the VIS-NIR region. The strongest absorbers in the NIR-SWIR region are water and lipids, but collagen also shows prominent absorption peaks [38]. The combination of these two spectrometers thus covers many of the important components of human and animal skin. Measurements over

24

this extended range of wavelengths provide more information than conventional DRS, and studies have shown that the ability to correctly quantify the content of water, lipids, and blood can be significantly improved [38]. It has previously been shown that this extended-wavelength DRS technique (EWDRS) can be used to accurately differentiate between healthy and metastatic human liver tissue [39, 40], to evaluate the degree of liver steatosis [41], and to monitor the perfusion in porcine eyelid flaps [35].

It is hoped that further development of this EWDRS technique will provide a tool for the non-invasive detection, classification, and delineation of skin cancers, that would not be dependent on the experience of the user. This was explored in a porcine model in the present work (Papers I and II).

Photoacoustic imaging

The purely optical imaging modalities in use today are able to provide information on the optical properties of tissue, but are limited by poor spatial resolution at greater depths due to strong light scattering. Although ultrasound imaging provides high spatial resolution in deep-lying tissues, it cannot provide functional contrast. Therefore, a technique combining optical imaging with ultrasound imaging would be advantageous.

Photoacoustic imaging is a novel non-invasive biomedical imaging modality that combines the advantages of optical and ultrasound imaging [42], thus being an optoacoustic technique. A laser unit emits nanosecond pulses of different wavelengths in the NIR region into the tissue. The energy of the pulses is absorbed by the tissue, leading to a slight increase in the temperature, which in turn results in ultrasonic signals due to thermoelastic expansion. These ultrasonic waves are collected by an ultrasonic transducer and converted into a multispectral image of the tissue. This enables high-resolution 3D images to be obtained showing the molecular composition of the tissue, to depths of a few cm into the tissue, thus having a clear advantage over purely optical methods [43]. An example of the images obtained is shown in Figure 5. The spectral PA signal of each pixel in the image is derived from the absorption of light by endogenous constituents of the tissue, such as hemoglobin, melanin, fat, and water. Exogenous contrast agents such as dyes or nanoparticles, have been added in some studies, making it possible to examine structures not otherwise visible with this technique, such as sentinel nodes [44].
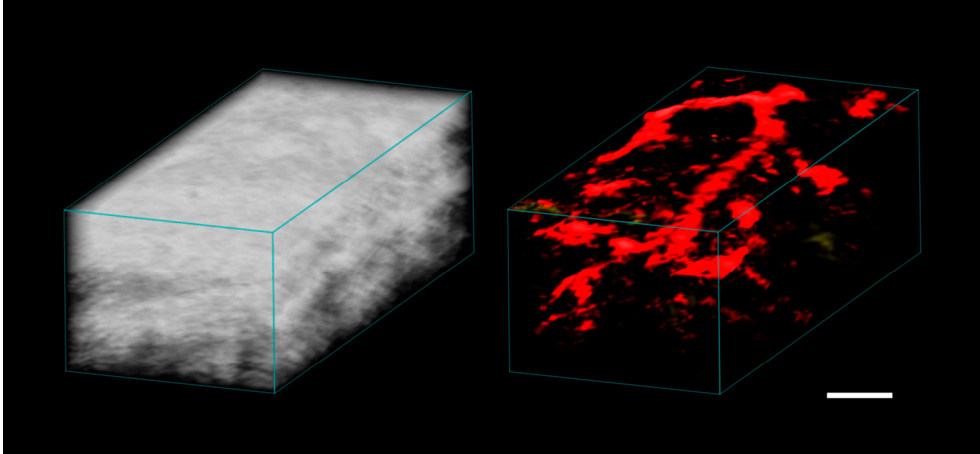
Figure 5. An example of 3D images obtained from a PAI examination of human skin *in vivo*. Left image shows the ultrasound image and the right shows the photoacoustic image, where the vascular network (red) is visible under the surface. Scale bar is 1 mm.

So far, PAI has mainly been developed experimentally, and only a few studies have been carried out on human skin tumors, mostly melanoma [45-54]. No studies have so far been carried out on eyelids; human or animal.

In the work presented in this thesis, PAI was used to study human BCC *ex vivo*, as well as the normal human eyelid *ex vivo*, and a case of eyelid BCC (Papers III, IV and V).

Machine learning methods for tumor classification

One of the drawbacks of many imaging techniques is that the data they produce must be interpreted. Most imaging techniques rely on subjective assessment, and a skilled examiner will thus obtain more reliable results than an unskilled user [23] [55]. Automated interpretation of the data obtained from images of skin tumors is thus desirable, so that the diagnosis would be reliable, regardless of the level of experience of the examiner. Machine learning methods could be useful in this context. Machine learning is an application of artificial intelligence in which software algorithms are designed and trained to learn from existing data, in order to make predictions based on future unknown data [56]. This is an emerging field within medicine, in which significant progress has been made at research level in recent years, providing promising results in several tasks, such as the classification of images. However, machine learning has not been implemented to any significant degree in the health care sector [57].

In the present work, a machine learning algorithm called a support vector machine (SVM) was assessed together with the EWDRS method (Paper I). SVM is commonly used within the field of medicine, for example, to classify cancers based on tumor markers in the blood [58], to interpret electroencephalography signals [59], to determine subgroups of schizophrenia [60], and to aid in decision-making in patients with symptoms of acute coronary syndrome [61].

Thesis at a glance

The studies described in this thesis are summarized in the table below.

Study	Aim	Method	Subjects	Site
I	To identify the optical fingerprints of different tissue types	EWDRS	Pigs	Three degrees of skin pigmentation, snout, tongue
II	To identify the borders of pigmented skin lesions	EWDRS	Pigs	Pigmented skin lesions
III	To differentiate between BCC and healthy skin	PAI	Patients	Excised BCC lesions
IV	To characterize the layers of the normal eyelid	PAI	Patients	Resected eyelids
V	To describe a case in which the BCC tumor margins could be determined perioperatively	PAI	Patient	Eyelid BCC

Aims

The aim of the work presented in this thesis was to evaluate two techniques for future non-invasive diagnostics of skin and eyelid tumors. A novel form of DRS with an extended wavelength range was evaluated *in vivo* on a porcine model, and PAI was evaluated *ex vivo* on human tissues.

The specific aims were:

- to study the ability of EWDRS to obtain optical fingerprints of different tissue types, and the use of machine learning techniques for automated tissue classification in pigs,

- to study the ability of EWDRS to identify the borders of pigmented skin lesions in pigs,

- to study the ability of PAI to differentiate between BCCs and healthy tissue in patients, and

- to study the ability of PAI to identify and visualize the layers of the normal eyelid and eyelid BCCs in patients.

Methods

Ethics

The animals used in the studies described in Papers I and II all received humane care in compliance with the European Convention on Animal Care. The experimental protocols were approved by the Ethics Committee for Animal Research at Lund University, Sweden.

All the patients participating in the studies described in Papers III, IV and V were given information about the study, and were informed of the voluntary nature of participation. All patients gave their fully informed written consent. The protocol for these experimental studies was approved by the Ethics Committee at Lund University, Sweden. The research was conducted in accordance with the Declaration of Helsinki as amended in 2013.

Animal preparation

Eight domestic pigs were used for the experiments described in Papers I and II. They were anesthetized and allowed to stabilize before the experiments were started. The flanks were shaved in order to allow skin measurements to be made. At the end of the experiments, the pigs were euthanized while still under general anesthesia. For a more detailed description, see the Methods section in Paper I.

Evaluation of extended-wavelength diffuse reflectance spectroscopy

EWDRS equipment

Diffuse reflectance spectral signatures were collected using a portable spectroscopic system comprising a contact fiberoptic probe, a tungsten halogen lamp providing a broadband spectrum from around 360 nm to 2000 nm, and two

spectrometers (Figure 6). The two spectrometers resolve light in the VIS-NIR wavelength range from 350 nm to 1100 nm, and in the NIR-SWIR region from 900 nm to 1700. All raw tissue spectra were background calibrated and intensity normalized. The overlapping wavelength region of the spectrometers (900 to 1100 nm) was used to combine the two spectra into a single continuous spectrum.
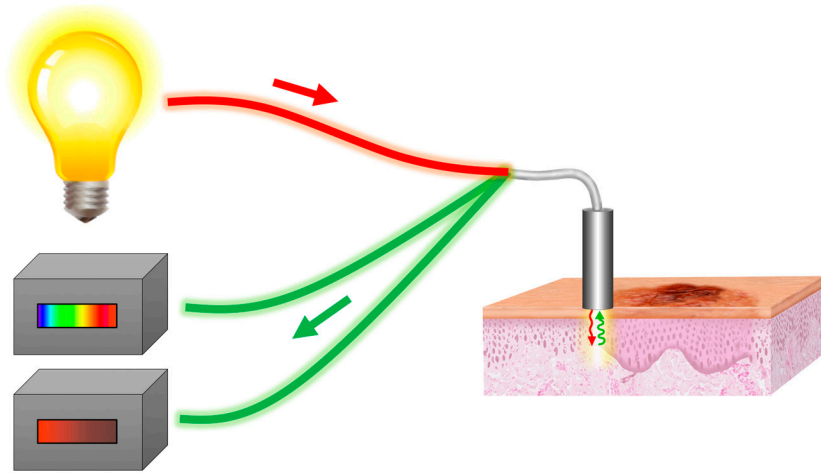

Figure 6. Schematic illustration of the EWDRS setup, with one light source and two spectrometers.

Two types of probe were used. In the study described in Paper I, the probe was a 10-mm-diameter fiber bundle consisting of a 10-fiber signal-collection ring around a single illuminating fiber with a source–detector separation of 2.5 mm. The final wavelength range was set to 450 to 1550 nm due to light source limitations, and to ensure a good signal-to-noise ratio. A finer probe was used in the second study (Paper II), with a 1.5 mm diameter, with a fiber bundle consisting of a 6-fiber signal collection ring around a single illuminating fiber, with a source–detector separation of 245 µm. In this case, a wavelength range of 350 to 1550 nm could be used due to the smaller source–detector distance.

Spectral signatures of different tissues

Five types of tissue were investigated in the study described in Paper I:

- non-pigmented skin on the flank,
- semi-pigmented skin on the flank,
- heavily pigmented skin on the flank,
- the snout, and
- the tongue.

EWDRS measurements were made at several different locations for each tissue type on each pig, and three to five consecutive recordings were made at each location. The average of these three to five measurements was used for further calculations. If the recordings appeared to differ significantly upon graphical visualization, they were discarded, as this indicated that the probe had not been held steadily. Twenty-eight recordings out of a total of 639 were discarded, resulting in 103 to 135 acceptable recordings for each tissue type.

Classification using machine learning

In order to be able to construct a classification model, the data were reduced using principal component analysis (PCA) with five principal components. Different types of machine-learning models were assessed, and a SVM using a quadratic kernel was found to give the best accuracy, and was therefore selected for further use. The method was validated using stratified five-fold cross-validation, meaning that the data were divided into five groups of equal sizes, and four of these were used to train the model, and the last one to test it. This was repeated for all folds, and the average test error was used to evaluate the model. The overall estimated accuracy was calculated, as well as the sensitivity and specificity for each tissue type in comparison to the others combined.

Identifying the borders of pigmented lesions

The main purpose of the study described in Paper II was to use EWDRS to identify the exact borders of pigmented skin lesions on pigs. The results were compared to those of histopathological analysis. The probe was held against non-pigmented skin and the signal was normalized to a flat line. The probe was then moved slowly towards the area of pigmentation by an operator who could not see the EWDRS signal. An observer who could not see the probe or the area of pigmentation monitored the EWDRS signal on a laptop. When the signal began to decrease distinctly the operator was notified, and the probe was pressed against the skin, leaving an impression. A needle was then inserted at that position (Figure 7). The lesion was excised and sent for histological examination. The distance between the point at which the needle was inserted and the histological border of the lesion was measured.
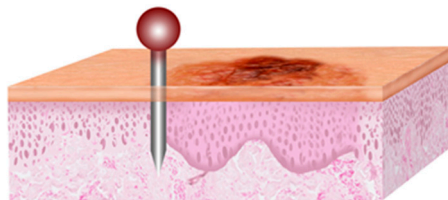

Figure 7. Schematic illustration showing how a needle was inserted to mark the border detected using EWDRS.

Evaluation of photoacoustic imaging

PA equipment

A photoacoustic system called the Vevo LAZR-X multimodal imaging system (FUJIFILM VisualSonics Inc., Toronto, ON, Canada) was used in the studies described in Papers III-V. This system allows simultaneous examination using ultrahigh-frequency ultrasound and PAI. Ultrasound imaging is used as a guide during PAI, and the ultrasound images are interleaved with the laser pulses. The system has an ultrasound transducer and a fiberoptic bundle coupled to a tunable laser. The laser is operated in the wavelength range 680 to 970 nm. Two planar light beams, located on either side of the ultrasound linear array, illuminate the skin surface. The photoacoustic waves are detected using an ultrasound linear array transducer (MX400), with a central frequency of 30 MHz and bandwidth of 22-55 MHz. Three-dimensional hybrid images of ultrasound and photoacoustic waves were obtained by scanning the transducer with a linear stepper motor, capable of step sizes between 40 and 500 μm, while capturing 2D images. The transducer-stepper motor arrangement is fixed on an adjustable arm to avoid motion artifacts caused by the examiner. A schematic of the PA setup is shown in Figure 8.
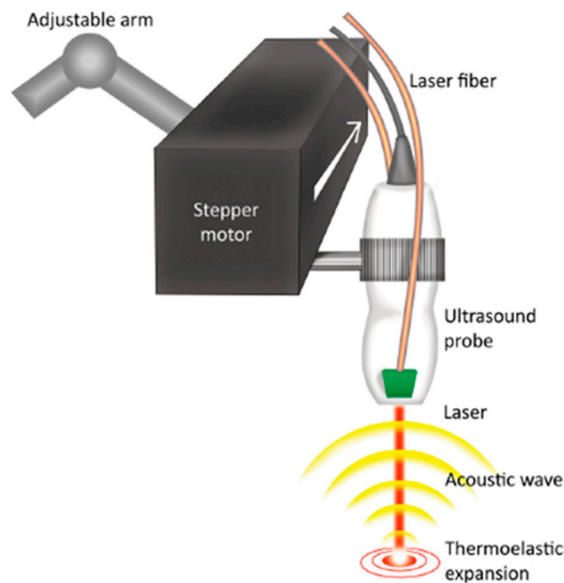
Figure 8. Schematic of the PAI setup. The PA probe consists of an ultrasound probe with laser fiberoptic bundles attached on either side. The tissue is irradiated with pulsed laser light, which causes thermoelastic expansion, which in turn generates acoustic waves that can be detected by the ultrahigh-frequency ultrasound probe. The PA probe is attached to an adjustable arm with a linear stepper motor to obtain a series of 2D images for the reconstruction of 3D images.

Safety aspects

The laser used in the PA system is a high-energy laser and it is thus very important to follow the relevant safety regulations. The system was set up in an examination room where windows and doors were covered according to laser safety regulations. For eye safety, protective block-out glasses were worn by the staff. During a PA investigation, both ultrasound and laser energy is used. Thus, if *in vivo* examinations were to be carried out, the patient is exposed to the energy from both the ultrasound probe and the laser. There are no standards or guidelines taking this combination into account, and those that exist for each of the modalities cannot be simply translated into guidelines for their combination. They can, however, be used as a guide, and in parallel with the work presented in this thesis, a study on the safety of the PA technique when making the clinical translation from an animal to a human setting has recently been published [62]. This study confirmed that it is safe to perform PA examinations on human skin *in vivo*. However, the energy supplied by the two modalities is too high to allow for examinations on, or in close proximity to, the eye.

Photoacoustic imaging of BCCs

The aim of the study described in Paper III was to investigate the properties of BCCs using PAI. Thirty-five patients, with 38 BCC lesions, recruited from the Department of Dermatology at Skåne University Hospital in Lund, were included for *ex vivo* investigation of their lesions. Six of the lesions were of the superficial subtype, 22 nodular and 10 morpheiform. The skin lesions were surgically removed under local anesthesia, according to standard clinical procedure. The lesions were then mounted in an acrylic container with an ultrasound-attenuating material on the bottom, filled with buffered saline solution (Figure 9).
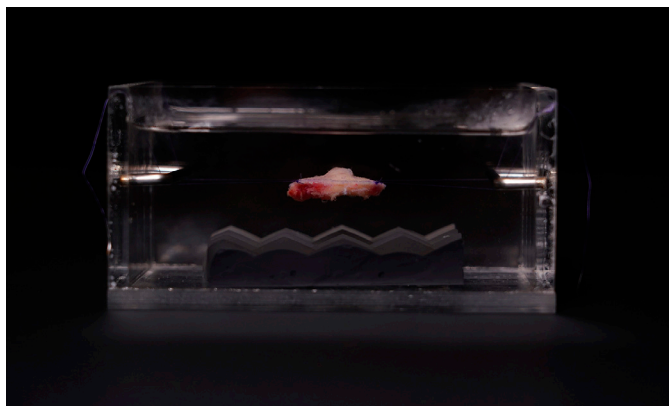

Figure 9. An excised lesion suspended in a saline solution in an acrylic container. An ultrasound-attenuating pad is placed in the bottom under the lesion.

Spectral signature of BCCs

Spectral scans were performed on each lesion: both on the lesion, and outside in healthy tissue, as a reference. A mean photoacoustic signature for all the tumors was then produced from these scans. This resulted in each 'pixel' of the ultrasound image having a PA spectrum dependent on the optical properties of the tissue.

Multiwavelength 3D scanning and spectral unmixing

The whole lesion was then scanned using the stepper motor. This generated a multiwavelength 3D scan, to which an imaging technique known as spectral unmixing was applied. Spectral unmixing uses the resulting mean BCC spectral signal obtained from the multiwavelength PA scans to produce a colored 3D image that maps the spatial distribution of a selected biological absorber, in this case, the tumor cells, by means of their distinct optical absorption spectrum. After *ex vivo* imaging, the lesion was placed in formalin and sent for histological analysis.

Photoacoustic imaging of the normal eyelid

Human resected eyelids were examined *ex vivo* using PAI, in order to characterize them (Paper IV). Nine patients, with either entropion, ectropion or trichiasis, who had been deemed suitable for horizontal lid-shortening surgery, were recruited from the Department of Ophthalmology at Skåne University Hospital in Lund. The patients underwent surgery under local anesthesia, according to standard clinical procedures. The Quickert procedure was performed on all the patients with entropion, where horizontal lid-shortening is combined with a transverse lid split and everting sutures [63]. Patients with ectropion underwent horizontal lid-shortening using either a pentagonal full-thickness resection in the area of maximum laxity, or a lateral margin wedge resection [64]. A total of 12 full-thickness eyelid resections were carried out. The resected tissue was then mounted in an acrylic container filled with buffered saline solution, with an ultrasound-attenuating material on the bottom of the container, as described above.

Spectral signatures of the tissue layers

Spectral 2D scans were made through the central portion of each resected tissue sample in the sagittal plane, thereby including all the layers of the eyelid. Regions of interest (ROIs) were defined by hand in the ultrasound image for the skin, orbicularis muscle, and the tarsal plate, and mean PA spectra of the three structures were then obtained by combining the signals from all 12 samples (Figure 10).
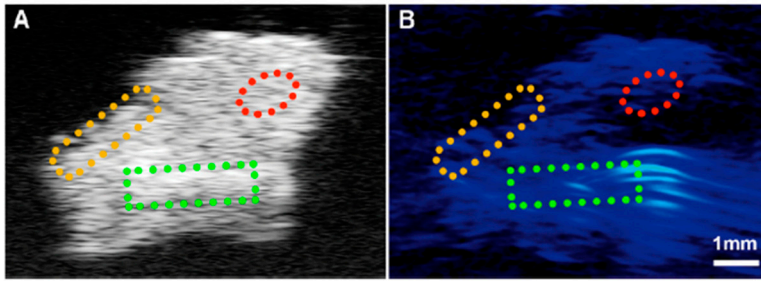
Figure 10. Representative example of a scan of an eyelid that was surgically removed using the Quickert procedure due to entropion. A) shows the ultrasound image and B) the PA image. ROIs were placed on the skin (orange), orbicularis muscle (red), and the tarsal plate (green).

Multiwavelength 3D scanning and spectral unmixing

A multiwavelength 3D image of each eyelid was acquired using the stepper motor, as described in Papers III and IV. Spectral unmixing was employed using the mean spectra for the different layers, resulting in a colored 3D image in which the eyelid skin, orbicularis muscle, and tarsal plate are visualized.

Photoacoustic imaging of a BCC on an eyelid

Paper V presents the case of an individual with a suspected BCC on an eyelid. An 87-year-old male presented at the Department of Ophthalmology at Skåne University Hospital in Lund with a suspicious 6 x 6 mm skin-colored lesion centrally on the left lower eyelid, of at least 6 months' duration. The tumor was surgically removed using a pentagonal excision procedure under local anesthesia, aiming at a surgical margin of 3-4 mm. The lesion was then placed in an acrylic container and examined using PAI. Both spectral 2D scans and a multiwavelength 3D scan were acquired.

ROIs were defined by hand in the ultrasound image, giving the spectral signal for the center of the tumor, and for healthy tissue, defined as the tip of the pentagonal excision. Spectral unmixing was employed using the tumor spectrum as reference, resulting in a colored 3D image where the tumor cell distribution is displayed. After PA scanning, the lesion was examined histologically for diagnosis and determination of the margins using standard hematoxylin and eosin staining. The tumor cell distribution according to PAI was compared to that obtained through histopathology.

Results and Discussion

Extended wavelength diffuse reflectance spectroscopy for tissue classification and margin identification

Spectral signatures for different tissue types

The results presented in Paper I showed that unique spectral reflectance responses could be obtained from the examination of five different porcine skin and tissue types with EWDRS, as shown in Figure 11. This indicates that EWDRS may also be able to differentiate between healthy skin and pathological skin lesions. When comparing the average EWDRS spectra for different skin types, it is clear that increasing pigmentation results in a decrease in signal amplitude in the lower part of the VIS-NIR region. This coincides with the absorption spectrum for melanin, the main chromophore responsible for pigmentation, as shown in Figure 12. The signals from the snout and tongue differ in that the tongue shows generally lower amplitudes in the VIS-NIR region. This is probably due to the fact that the tongue is a muscular organ that contains high amounts of myoglobin and blood. The main chromophore of blood is hemoglobin, which exists in two forms, oxygenated and deoxygenated, both of which are strong absorbers in this wavelength region.
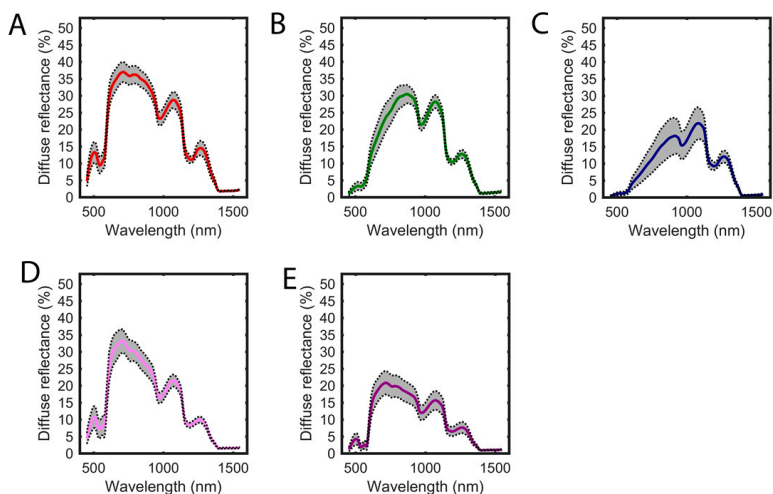

Figure 11. The average diffuse reflectance curves for the different porcine tissues investigated: A) non-pigmented skin, B) semi-pigmented skin, C) heavily pigmented skin, D) snout, and E) tongue. The standard deviation is indicated by the gray shading.
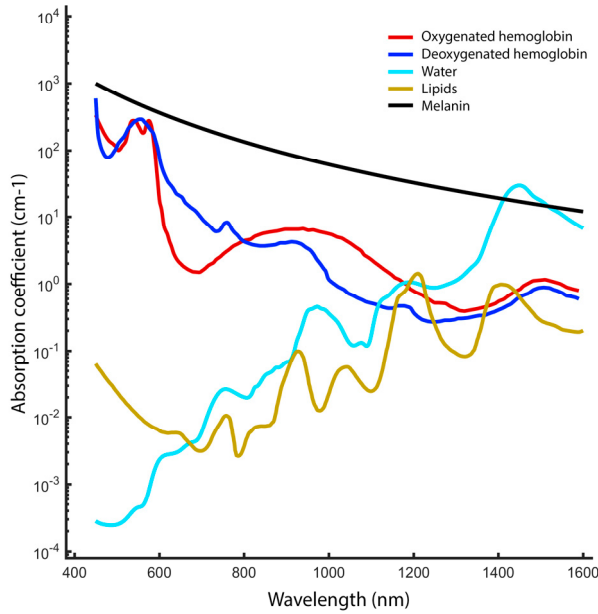
Figure 12. The absorption spectra of the dominant intrinsic absorbers in biological tissue in the wavelength range covered by the EWDRS system. Adapted from [65].

In general, each type of tissue gives rise to a different reflected spectrum depending on the type and amount of molecules in that tissue. Different chromophores absorb the incoming light differently, and the size and density of the molecules affect the scattering of the light. This results in a unique optical "fingerprint" for each kind of tissue examined. In order to obtain as much information as possible, the EWDRS device was constructed to collect a very stable signal from 450 to 1550 nm, using a single probe. Using this device, it was found that each skin and tissue type studied exhibited a unique spectral signature. This is in line with previous studies showing that DRS could be used to determine properties such as the hemoglobin and melanin concentration in skin [66], the oxygen saturation in skin flaps [67], and to classify breast cancer biopsies [68], by collecting spectra in the UV-VIS or the VIS-NIR region. Other studies have focused on the SWIR region, where water, lipids, and collagen are strong absorbers [69]. This EWDRS device thus shows potential for the detection of differences in tissue due to pigmentation, as in the case of malignant melanomas, and other, more subtle differences in tissue composition, as in the case of BCC or SCC, compared to healthy skin.

Classification of tissues using machine learning methods

The EWDRS spectra from the five kinds of porcine tissue were transformed using PCA with five principal components to enable further analysis. This resulted in every spectrum being transformed into a data point in five dimensions, from which the first three is displayed in Figure 13. Visualizing the measurements in this way, it becomes obvious that they appear in clusters with little overlap and that it should be possible to classify them by some means. For this task, a support vector machine (SVM) with a quadratic kernel was trained using this set of data.
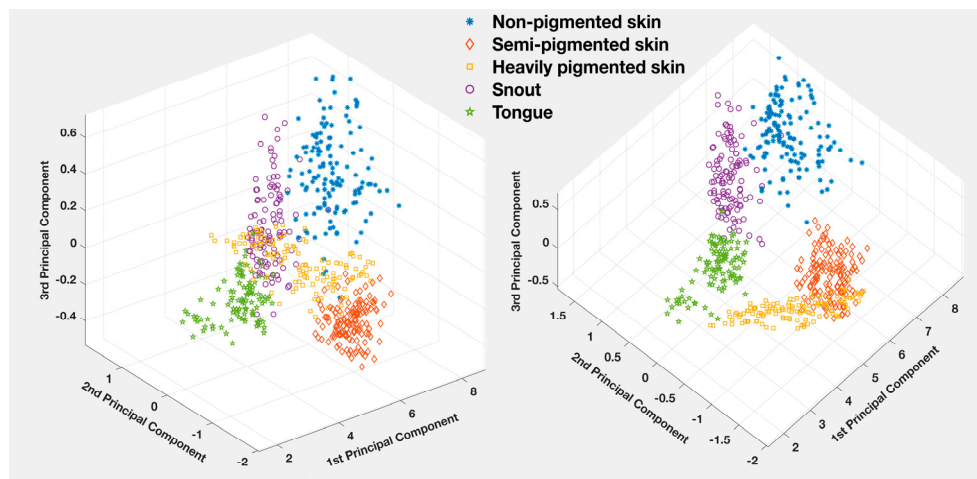

Figure 13. The EWDRS measurements at two different angles using the first three principal components after PCA. The five different tissue types appear as clusters with little overlap.

The setup described in Paper I had an overall accuracy of 98.2%. The performance of this classification model, expressed in terms of sensitivity and specificity for each type of tissue, were all between 96.4 and 99.8%. These results show that EWDRS together with a machine learning method, SVM, had the capability to identify the kind of tissue being examined. Tissue identification was completely automated, and required no user experience. Further development of the software will hopefully allow identification to be made instantly.

The EWDRS technique thus seems to be a promising tool for the rapid, non-invasive diagnosis of skin lesions such as skin tumors. However, detailed studies on tumor tissue and the surrounding healthy tissue are required, followed by clinical trials. It would be of great value to be able to correctly diagnose and pre-surgically define the tumor margins of malignant melanomas and non-pigmented skin lesions such as basal cell carcinomas, squamous cell carcinomas, and actinic keratosis.

Identifying the borders of pigmented skin lesions

The same EWDRS setup was evaluated to investigate its ability to delineate pigmented lesions on porcine skin (Paper II). To obtain as accurate readings as possible, a finer 1.5-mm-diameter probe was used. A characteristic decrease in the 350-800 nm range was observed when moving the probe from non-pigmented skin to the pigmented lesion. The distance between the EWDRS-defined border and the histological border was measured (Figure 14), and the median difference was found to be -70 µm, meaning that the EWDRS-defined border was, on average, 70 µm further into the pigmented area than the histologically defined border (range -579 to 538 µm, n = 13).
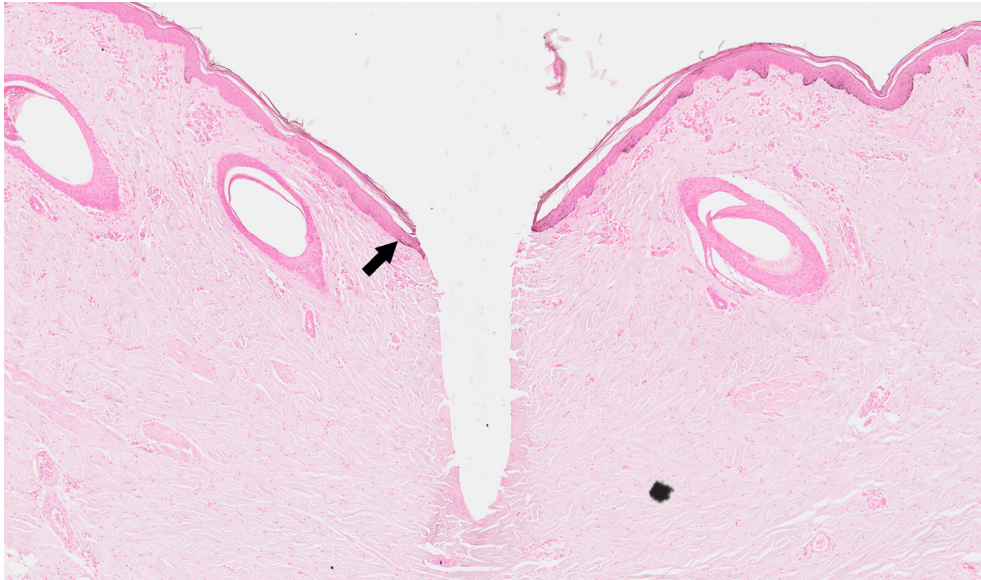

Figure 14. Histological cross-section showing the hole where the needle was inserted and the histologically defined border between pigmented and non-pigmented skin (black arrow).

A difference of this order of magnitude can be considered a good result, compared with existing practice, in which the surgeon estimates the border by visual inspection. Even after adding another 3-6 mm of clinically uninvolved margin before excision, as in the case of BCCs, a significant proportion of excisions show positive margins, requiring reoperation [70]. Using EWDRS to define the histological border with the same precision as that reported in Paper II, and adding a further margin of 4 mm would probably yield a better rate of radical excision.

Malignant melanomas contain large amounts of melanin, and similar changes in the EWDRS signal when moving from healthy tissue to the tumor, would probably be seen as when moving from non-pigmented porcine skin to pigmented skin.

BCCs and SCCs do not usually contain more melanin than the surrounding tissue, which means that differences in the signals from healthy tissue and the tumor would have to depend on other differences, such as molecular composition. Skin tumors are often more highly vascularized [71] and exhibit differences in lipid profile [72] [73] and collagen composition [74], compared to normal tissue. These dissimilarities should lead to differences in the signals from such tumors, however, studies must be performed on human lesions to confirm this.

A limitation in the use of EWDRS to delineate tumors preoperatively, is its small measuring depth. The penetration depth depends foremost on two factors: the wavelengths being used and the distance between the emitting and receiving optical fibers [75]. Light with shorter wavelengths has a shorter penetration depth, while longer wavelengths penetrate further into the tissue. Similarly, a greater emitter–receiver fiber distance results in deeper measurements, but at the expense of resolution. EWDRS is thus not suitable for determining the depth of skin tumors, and other techniques must be used, such as high-frequency ultrasound or PAI. Another problem that must be solved before the technique can be used for tumor margin detection in the clinical setting is that a means must be found of making some kind of mark on the skin indicating the tumor border. A thinner probe was used in the second study, not only to obtain more exact location of the border, but also to allow a small impression to be made on in the skin, indicating the tumor border. In the future it would be helpful to design a probe with a built-in system for indicating this exact position with ink, making it possible to map out the tumor distribution step by step prior to surgery. Furthermore, better software would allow user-independent, real-time interpretation of the collected signal, indicating whether the tissue is cancerous or not. The user would require no specific histological knowledge, as is the case with many of the other modalities described in the introduction.

Photoacoustic imaging for the characterization and visualization of basal cell carcinomas

Defining the spectral signature

The study described in Paper III was designed to investigate the typical PA signal of a human BCC *ex vivo*. A clear difference was found between the mean spectrum from BCCs and that from healthy tissue, as can be seen in Figure 15. This difference was analyzed statistically, and was statistically significant (p <0.05) in the wavelength range 760-945 nm.
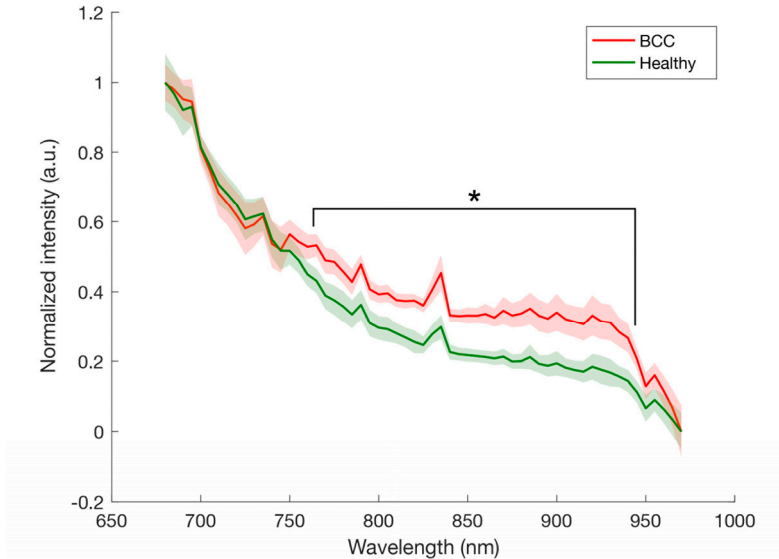
Figure 15. The mean PA spectra obtained from BCCs and the surrounding healthy tissue from *ex vivo* measurements. The dispersion (± one standard deviation) is indicated by the shaded areas. A clear difference can be seen in the spectral signatures of the BCCs and healthy tissue ($p<0.05$ for 760 to 945 nm, n=38).

Different kinds of BCCs (superficial, nodular, and morpheiform), were included in this study, reflecting the pattern commonly seen in the clinical setting. It is possible that different subtypes of BCC have different spectral signals, but the material available in the present study was too small to be able to detect such a difference statistically. This must therefore be explored in a larger study, including more BCCs of each subtype.

This study is probably the first to examine the PA spectral fingerprint of BCCs. A few other studies have investigated BCCs, but were mostly concerned with pigmented BCCs [48, 49], which are uncommon in the Caucasian population [76]. Pigmented BCCs contain melanin and thus have different optical properties from non-pigmented ones, and should therefore demonstrate similarities to MM or benign nevi. Other groups have examined non-pigmented BCCs and SCCs [77], but only measured the PA signal at a specific wavelength. Obtaining spectra over a range of laser frequencies from 680 to 970 nm, as in the present study, offers a better opportunity to find and highlight differences between skin tumors, for instance, and healthy tissue.

44

Three-dimensional visualization

Three-dimensional scans were obtained by scanning the excised lesions using the stepper motor (Paper III). Spectral unmixing was performed using the previously calculated mean absorption spectrum for BCCs. This gives a 3D map of the distribution of typical tumor cells. Figure 16 shows a spectrally unmixed 3D sequence from a tumor examined *ex vivo*, illustrating how this can be used to differentiate tumor cells from the surrounding healthy tissue.
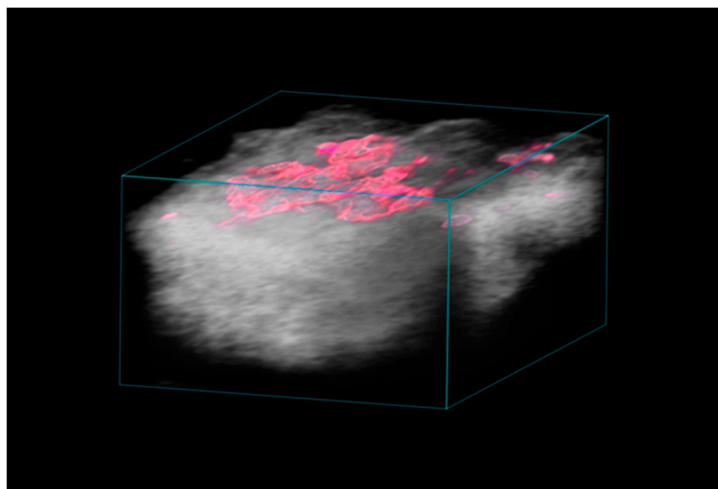

Figure 16. Representative example of a spectrally unmixed 3D multiwavelength PA image of a BCC lesion examined *ex vivo*. Cancerous cells are shown in pink.

This demonstrates that it is possible to image the 3D distribution of BCC cells. In this case, the tumor was examined *ex vivo*, after surgical excision, but preoperative *in vivo* scanning should also be feasible. Further development of this technique may make it possible to scan a tumor before surgery to guide the surgeon in its excision. As PAI not only provides information of surface structures, but can penetrate several centimeters into tissue, it would be possible to map out not only the lateral boundaries, but also the depth of the tumor. As with the EWDRS technique described in Papers I and II, it would be very useful to integrate an ink marking system into the probe, to mark out the tumor borders on the skin surface.

Another possibility may be to scan the excised lesion perioperatively, during surgery, to check whether the margins are free from tumorous cells. If not, further excision can be performed until PAI shows that the whole tumor has been removed, similar to the procedure in Mohs surgery.

So far, only a few other research groups have used PAI to study the size of BCCs, mainly their depth [45, 48, 49, 77]. A research group in Singapore has shown that PAI can be used to visualize and measure the depth and length of BCCs *in vivo* in

a small group of patients [49]. Their 3D reconstructions were made using 10 wavelengths between 700 and 900 nm with an inVision 512-echo optoacoustic imaging system (iThera Medical, GmbH, Munich, Germany) [45, 49]. The majority of the patients in their study presented with pigmented BCCs, and the tumor depth and length were obtained by calculating the distance between the non-baseline values of the melanin signals after spectral unmixing.

Most clinical *in vivo* and *ex vivo* studies using PAI have been performed on melanoma lesions [46, 47, 52, 54, 78]. Melanoma lesions contain high amounts of the endogenous chromophore melanin, which has a known absorption spectrum [79]. The patients included in the study described in Paper III were defined as Fitzpatrick skin type I or II (i.e. fair-skinned), and none had a pigmented BCC. The study described in Paper III shows that it is possible to use PAI to identify and visualize tumors based on bio-optical properties that do not rely on differences in melanin concentration.

Photoacoustic imaging for the characterization and visualization of the human eyelid

Defining the spectral signature of the normal layers of the eyelid and 3D visualization

The results presented in Paper IV show that the mean PA signatures for the eyelid skin, the orbicularis muscle and the tarsal plate could be measured *ex vivo*. A significant difference was found between the signals from the tarsal plate and the orbicularis muscle, and between the skin and the orbicularis muscle. However, no statistically significant difference was found between the skin and the tarsal plate. The reason for this could be that the muscle contains a considerable amount of myoglobin, and is a well-perfused structure with a relatively high amount of blood, even when excised. Myoglobin, and hemoglobin, in both its oxygenated and deoxygenated state, are strong absorbers in the wavelength range 680 to 970 nm [80] [81]. The skin and tarsal plate, however, contain less blood, and consist mainly of connective tissue. The tarsal plate contains collagen fibers, whereas the skin consists primarily of keratinocytes, which manufacture and store the fibrous protein keratin, and a mesh of elastin and collagenous fibers [82].

The application of spectral unmixing to the multiwavelength 3D sequence revealed the overall architecture of the eyelid and the distribution of skin, the orbicularis muscle, and the tarsal plate (Figure 17). No studies have hitherto been published on the imaging of eyelids or periorbital tissue in humans or animals using PAI. This region contains several anatomical structures that interact with

each other to keep the eye lubricated and protect it from the outer world. It is important to be able to characterize the structure of the eyelids and the tissue around them in order to be able to distinguish between healthy and diseased tissue, so as to spare as much healthy tissue in the eyelids as possible.
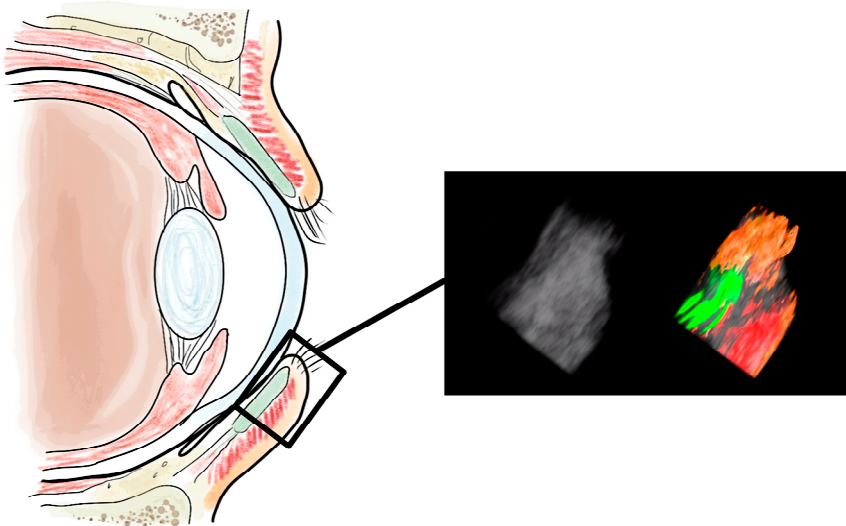

Figure 17. A representative example of the 3D ultrasound image obtained from a full-thickness sample from a lower eyelid resected due to entropion using the Quickert procedure. The ultrasound image shows hardly any structures within the eyelid, but several structures can be identified when the spectrally unmixed PA signal is overlaid. Orange: skin, red: orbicularis muscle, green: tarsal plate.

The PA equipment used in the studies described in this thesis includes a high-energy laser, which makes measurements on, or in the proximity of, the eyes impossible. It would probably not be safe to use the equipment even when using light-blocking corneal shields to prevent the laser from entering the cornea and lens and being focused onto the retina, due to light propagating through the surrounding tissue into the eye. Future PAI units intended for *in vivo* use in the periorbital area, or even on the eye itself, would have to be equipped with a function that allows the energy of the laser to be reduced.

Surgical margins of basal cell carcinomas on the eyelid

Paper V presents the case of a patient with a BCC on the left eyelid. After resection, the lesion was scanned *ex vivo* using PAI. After performing 3D reconstruction and spectral unmixing, the tumor was seen not only centrally, as expected, but tumor cells were also seen all the way out to the medial margin

(Figure 18A). This indicated that excision had probably not been radical, and subsequent traditional histopathological examination indeed revealed an intermediate/infiltrating BCC, and confirmed that excision was not complete in the medial region (Figure 18B).
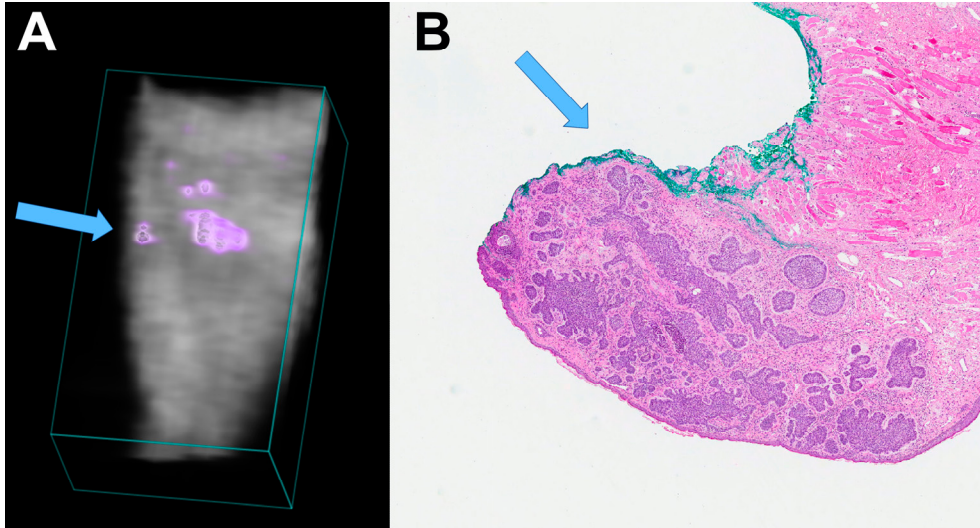

Figure 18. A) Spectrally unmixed 3D multiwavelength PA image of the pentagonal excision showing BCC cells as a purple overlay. B) The hematoxylin- and eosin-stained histological image of the eyelid with the BCC, where the medial edge of the resection is colored green. The presence of tumor cells in the margin of the sample (blue arrows) shows that excision was not radical.

If the more remote cancer cells had been identified perioperatively using PAI, it would have been possible to perform a radical excision before reconstructing the eyelid defect, sparing the patient further surgery. However, larger human studies are required to confirm that the sensitivity and specificity of PAI are sufficiently good to ensure radical, but normal-tissue-sparing excision, before the technique can be used in the clinic.

The automatic diagnosis and delineation of skin tumors could be based on large datasets of *ex vivo* PA measurements on biopsy-verified tumors from thousands of patients. Datasets covering differential diagnoses, such as BCC, SCC, actinic keratosis, and sebaceous carcinoma, as well as more benign lesions, could be used. If successful, automatic PAI could become a useful and reliable alternative to conventional microscopic histology for use in Mohs surgery. The advantages are that there would no longer be a need for a skilled pathologist, and the examination time would be faster, as the tissue could be examined directly after excision, without any need for histological preparation.

Conclusions

Extended-wavelength diffuse reflectance spectroscopy

It was shown in this work that EWDRS could be used *in vivo* to differentiate between different skin and tissue types in a porcine model with excellent specificity and sensitivity. This was done by employing a machine learning technique, SVM, that provided skin and tissue type classification with an overall accuracy of over 98%. EWDRS could also be used to non-invasively define the border between pigmented skin lesions and the surrounding non-pigmented with good accuracy. The examinations were performed with a hand-held probe and took only a few seconds. Using appropriate software, the signal could be analyzed in real time to provide a non-observer-dependent diagnosis using machine learning. Future studies are needed to validate the method on human skin tumors. Hopefully, further development of this technique will lead to a diagnostic tool for non-invasive tumor classification and margin delineation.

Photoacoustic imaging

The spectral signals from PAI showed statistically significant differences between BCCs and healthy tissue in an *ex vivo* setting. Spectral unmixing allowed the tumor cell distribution and overall lesion architecture to be visualized in 3D. PAI could also be used to characterize the PA spectra of the different layers in the human eyelid *ex vivo*. The eyelid skin, orbicularis oculi muscle and tarsal plate could be visualized in 3D using spectral unmixing. PAI was employed in a case study where an eyelid BCC was examined directly after excision and visualized in 3D. This PA examination indicated that the excision was non-radical, and subsequent histopathological examination confirmed this. These results indicate that PAI could be used to visualize and delineate tumors on the skin, including the periorbital region. After further development, the technique could hopefully help in guiding surgical intervention to achieve more precise excision of skin cancer with better clearance, reducing the need for repeated surgery. Another possible application of PAI is the rapid examination of freshly excised unfixed tissue during surgery, to determine whether excision has been radical, or if further

excision is necessary. This would not only save time compared to conventional microscopic histology, but also reduce the need for further surgery.

Challenges and Future Outlook

Both the imaging modalities evaluated in this research showed that there is potential to improve the diagnosis and delineation of skin cancer compared with the methods currently employed. However, several obstacles must be overcome before they can be applied in everyday clinical practice.

Investigations must be performed to establish whether EWDRS can be used to identify different kinds of human skin tumors through their spectral signatures. Our group has performed a small pilot study, showing promising results, and larger studies are planned. While it can sometimes be an advantage to investigate a skin tumor using a thin probe in order to map out the extent of the tumor point-by-point, in most cases an instant 2D image of the tumor would be preferable. A hyperspectral camera will therefore be included in our future studies of skin tumors. This will make it possible to obtain hyperspectral images of larger areas that can be analyzed using principles similar to those used in EWDRS. One drawback of EWDRS and hyperspectral cameras is that they only provide information on the surface of the examined tissue, and cannot be used to determine the tumor depth. It is thus necessary to combine EWDRS with another technique that penetrates deeper into the tissue to obtain information on tumor thickness. PAI is one such technique.

PAI was used to study BCCs and healthy eyelids *ex vivo*. Studies by our group on other kinds of skin cancers, such as SCCs and MM are ongoing, and have been broaden to include the study of tumors *in vivo*. Larger *ex vivo* studies are also ongoing regarding eyelid tumors (mainly BCC, SCC, and MM). One of the challenges associated with examining skin tumors *in vivo* with PAI is that motion artefacts reduce the quality of the images. Measures have already been taken to stabilize the patient and the examination area as much as possible, and further work is being carried out to further reduce motion artifacts using a technique called motion tracking.

The PAI system used in this work (Papers III-V) can also provide laser energies between 1200 and 2000 nm, which would allow the visualization of chromophores other than those visible in the range 680-970 nm. However, this would require considerable development, as standard ultrasound coupling medium absorbs most of the energy at these wavelengths, and little radiation would therefore reach the skin surface. Work has started on investigating whether other, less absorbing,

substances could be used as ultrasound coupling media. Further improvements are required in methods of tissue classification, and a means must be found of reducing the laser output so that PAI could be safely used for *in vivo* examination of the eyelids.

Populärvetenskaplig sammanfattning

Hudcancer är väldigt vanligt bland befolkningen och beror ofta på solens UV-strålar. Den absolut vanligaste formen kallas för basalcellscancer, eller basaliom, vilken visserligen nästan aldrig sprider sig till andra platser men som däremot kan förstöra vävnaderna där den växer. En annan form är malignt melanom, som kan sprida sig ut i kroppen och leda till döden. Standardmetoden för behandling är operation och tillvägagångssättet har inte ändrats nämnvärt de senaste årtiondena. Ofta görs en visuell uppskattning av tumörens utbredning av kirurgen, som också lägger till några millimeter för att få lite extra marginal. Efter operationen skickas preparatet för mikroskopisk granskning hos patologen. Där fås den slutgiltiga diagnosen och också information kring huruvida tumören verkar vara borttagen i sin helhet eller om det finns tumörceller ända ut till kanten av den bortskurna vävnadsbiten. Om cellerna sträcker sig ända ut hit är det troligt att det också finns celler kvar i huden och då är risken överhängande att tumören på nytt kommer att börja växa. Därför innebär detta att det krävs ytterligare minst en operation där mer vävnad tas bort på samma sätt.

Ibland kommer svaret istället att det som för blotta ögat såg ut som cancer i själva verket var frisk vävnad när det granskades mikroskopiskt. I detta fall innebär det att operationen var onödig och att frisk hud opererades bort.

Ögonlocken är solutsatta och drabbas därför också ofta av hudcancer, främst basaliom. Här är det ännu viktigare att hela tumören tas bort och att frisk vävnad inte offras i onödan. Detta eftersom den rekonstruktiva kirurgin, d v s återställandet av ögonlocket och dess funktion, blir mer avancerad ju mer vävnad som tas bort. Dessutom blir det allt mer svårt att få till ett kosmetiskt acceptabelt slutresultat.

Olika tekniska metoder har testats genom åren för att försöka förbättra precisionen med vilken tumörerna kan kartläggas före operationen, men ingen har varit tillräckligt bra för att slå igenom i den kliniska vardagen.

I denna avhandling testas två nya tekniker för att diagnostisera och avgränsa hudtumörer: diffus reflektansspektroskopi med utökat våglängdsspektrum (på engelska *extended wavelength diffuse reflectance spectroscopy*, förkortat EWDRS) och fotoakustisk avbildning (på engelska *photoacoustic imaging*, förkortat PAI).

I Studie I och II utvärderades EWDRS i en grismodell. Diffus reflektansspektroskopi är en välkänd metod där ljus skickas in i vävnaden och det som kommer tillbaka analyseras och ger ledtrådar om vad vävnaden består av. I vår forskargrupp har vi vidareutvecklat detta genom att bygga ihop ett system som kan analysera ljus i ett utökat våglängdsområde och därigenom borde mer information från vävnaden kunna fås fram.

Syftet med Studie I var att se om EWDRS kunde se skillnad mellan fem olika vävnader. Mätningarna gjordes och med hjälp av maskininlärning (en gren av artificiell intelligens) gick det att med hög precision låta datorn berätta vilken av de fem vävnaderna som ljuset riktades mot. Förhoppningsvis går det att i framtiden utveckla tekniken så att det på samma sätt går att se skillnad på frisk hud och olika typer av hudtumörer.

I Studie II testades EWDRS för att se om tekniken kunde användas för att hitta gränsen mellan pigmenterade hudförändringar och omkringliggande hud. Ljuset skickades in i vävnaden med hjälp av en tunn prob (Figur 19) och det gick att se att signalen ändrades när proben kom till gränsen till hudförändringen. Via mikroskopisk undersökning gick det sedan att se att vi med hjälp av EWDRS kom mycket nära den faktiska gränsen. Detta medför att vi tror att tekniken skulle kunna utvecklas för att kartlägga gränserna för olika hudtumörer, vilket kan vara till stor hjälp för kirurgen inför operationen.


Figur 19. Diffus reflektansspektroskopi. Ljuset kommer in via en tunn prob och förs sedan tillbaka via samma prob till analysutrustningen.

I studie III, IV och V testades PAI på mänsklig vävnad. PAI är en ny teknik som hittills främst använts experimentellt på djur. Vid fotoakustiska mätningar skickas det in starkt laserljus i vävnaden och detta ljus absorberas av de olika molekylerna

som finns där inne. Detta leder till en liten värmeökning som i sin tur gör att molekylerna vibrerar och det utsöndras ett litet ultraljudseko. Ultraljudet som bildats kan sedan mätas med utrustningen och kan översättas till en tvärsnittsbild av vävnaden som sträcker sig flera centimeter ner på djupet.

Syftet med Studie III var att göra mätningar på basaliom. Patienter som skulle opereras för detta på hudkliniken på Skånes Universitetssjukhus i Lund deltog. Direkt efter att tumören opererats bort gjordes fotoakustiska mätningar på vävnadsbiten. Resultatet visade att tumören och den friska vävnaden runt omkring gav olika fotoakustiska signaler. Detta gjorde att det också gick att skapa tredimensionella bilder av vävnaden där tumörcellernas utbredning kunde visas i tydliga färger (Figur 20). Vi hoppas därför att PAI i framtiden ska kunna användas till att avbilda tumörer både innan operationen, men även under operationen, för att se om hela tumören verkar blivit borttagen.
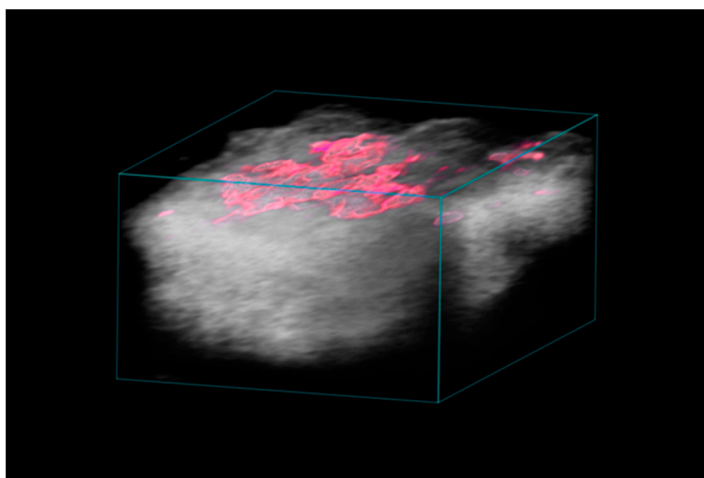
Figur 20. Tredimensionell fotoakustisk bild där tumörvävnaden givits rosa färg för att synas mot den omkringliggande friska vävnaden.

I Studie IV användes PAI för att mäta på och avbilda delar av ögonlock som opererats bort. Resultatet visade att det gick att identifiera ögonlockets olika lager och visa upp dessa i tre dimensioner. I Studie V undersöktes ett preparat där ett basaliom beläget på ett ögonlock opererats bort. Med hjälp av tekniken gick det att visa att tumören sannolikt inte var bortopererad i sin helhet, vilket bekräftades av den sedvanliga mikroskopiska undersökningen hos patologen.

Sammanfattningsvis verkar både EWDRS och PAI lovande men det behövs ytterligare forskning innan de kan komma att användas i den kliniska vardagen på våra sjukhus.

Acknowledgements

Aldrig förr har en Ulf haft så många att tacka för så mycket.

Jag har haft turen att hamna i en fantastisk forskargrupp som är kreativ, dynamisk och med en aldrig sinande ström av spännande idéer att utforska (och motsvarande tidsbrist). Det är en grupp där alla alltid ställer upp för varandra och det är något jag önskar att alla doktorander skulle få uppleva. Min forskning har innefattat allt ifrån klassiskt forskningsarbete såsom planering, experiment, databearbetning och manusförfattande, till mindre klassiskt dito som involverat slagborr, skruvdragare och äventyrliga förflyttningar av dyra och tunga prylar. Den här tiden har varit något utöver det vanliga!

Min forskarkarriär är tätt sammankopplad till min kliniska karriär som ögonläkare vid Ögonkliniken SUS Lund/Malmö. Jag förstod tidigt under grundutbildningen att ögonsjukdomar och ögonkirurgi var det roligaste man kunde hålla på med. Det var många som bidrog till att jag fick in en fot på Ögonkliniken och ännu fler som var välkomnande och hjälpsamma under min första tid här. För detta är jag evigt tacksam. Det är fantastiskt att vara på en arbetsplats som består av ett myller av vänner.

Ett stort tack till er alla som särskilt nämns nedan men även alla andra som bidragit i stort och smått.

…

Malin Malmsjö, huvudhandledare och professor. Hon besitter lika mycket energi som ett medelstort kärnkraftverk och delar frikostigt med sig av denna. Idéer som för mig framstått som nästintill omöjliga att genomföra har inom loppet av några veckor eller månader blivit till verklighet. Hon är något så ovanligt som en jordnära visionär som har en avundsvärd förmåga att på ett strategiskt, insiktsfullt och målinriktat sätt få igenom det mesta. Hon är alltigenom en inspiratör som har lärt mig massor. En bättre handledare hade jag inte ens kunnat föreställa mig.

Jonas Blohmé, bihandledare, ögonplastik- och skelningskirurg. Min kirurgiska mentor och främsta förebild med så stora tofflor att de nog aldrig kommer att gå att fylla. Han har en häpnadsväckande förmåga att dra vitsar, sjunga, dansa och operera – samtidigt. Trollbinder sina patienter medelst konversation så till den grad att det är tveksamt att det egentligen hade behövts något annat bedövningsmedel.

Karl Engelsberg, bihandledare, ögonplastikkirurg. Kirurgisk mentor som med sin kunnighet, hjälpsamhet och ihärdighet är en stor inspirationskälla både för mig och många andra på kliniken. Hans kontinuerliga stöd har betytt mycket genom åren.

Nina Reistad, bihandledare, atomfysiker. Ljusets härskarinna som inte har några problem med att se saker i tio dimensioner när vi vanliga dödliga får nöja oss med tre. Har fått mig att inse att fotoner är luriga rackare som gillar att rymma. Kommer ofta med kloka synpunkter som inledningsvis känns besvärliga men som alltid visar sig vara korrekta.

Rafi Sheikh, min kumpan och vapendragare inom forskningen och mycket annat. En framåtsträvande, energisk, optimistisk realist som aldrig tycks behöva sömn. Säger bara precis som det är, utan filter, oavsett sammanhang. På gotländska.

Cu Dybelius Ansson, min favoritbokstav i alfabetet som med all säkerhet kommer att bli nästa stjärna inom glaukomkirurgin. Rakryggad som få med mängder av intressanta infallsvinklar på alla tänkbara samtalsämnen.

Khashayar Memarzadeh, a k a Khash. Mannen med det coolaste smeknamnet (bra mycket bättre än de jag brukar få dras med för övrigt). Kirurg med många strängar på sin lyra. Var delaktig i många av våra experiment varifrån jag fått många minnen jag aldrig kommer att glömma.

Björn Hammar, hela Sveriges neurooftalmolog. Pedagogisk förebild med lysande föreläsningar, trots märklig brytning (pratar huvudstadska). Sägs, från säker källa, ha goda sidor också. Jag tror till och med att de är många.

Josefine Bunke, vår utpost i Växjö som är nästan obehagligt effektiv och självgående. Jag tror att vi är många som hoppas att hon en dag ska ta sitt förnuft till fånga och flytta ner hit istället.

Magdalena Naumovska, en mycket klipsk kollega som ägnar sig mycket åt ögats bihang (hjärnan). Kan verka oskyldigt charmig och social men tvekar inte att dra folk i öronen när så behövs.

Jenny Hulth, kollega som lagt ner mycket tid och engagemang i vårt gemensamma tumörprojekt. Hon är en doer ända ut i fingerspetsarna och en mycket god handledare för både studenter och andra.

John Albinsson, vår in-house forskningsingenjör med spetskompetens inom ultraljud. Jag påstår inte att han är vår frälsare, men vår tideräkning är indelad i "före John" och "efter John". Har förmågan att genomföra en komplex uppgift på utsatt tid trots tusen störningar från oss andra – med ett bibehållet glatt humör dessutom.

Aboma Merdasa, headhuntad ingenjör som nyligen börjat i gruppen. Problem som jag gått och funderat på i flera år löste han på några dagar. Men jag är inte bitter.

Bertil Persson, överläkare hudkliniken i Lund. Ovärderlig kontakt på hudkliniken som kommer med många insiktsfulla idéer och tankar och som har gjort det möjligt att ha ett så fint samarbete mellan ögon- och hudkliniken.

Magnus Cinthio och **Tobias Erlöv**, ljudets furstar på LTH. Bidrar enormt med sina ultraljudskunskaper. En duo som kan konsten att dyka ner i oerhört svåra problemfrågeställningar och sedan dyka upp igen och göra något vettigt av det hela.

Johanna Berggren, kollega på plastikkirurgisidan som inte räds för att jobba hårt. Hängiven sitt yrke och mästare på forskningslogistik.

Kajsa Tenland, skelningskollega med härlig humor. Kan tygla de mest bångstyriga och misslynta barnen.

Rannveig Linda Thorisdottir, kollega som delar min smått besynnerliga fascination för att skära både i folks ögonlock och i deras ögonmuskler. Vi borde bilda en klubb.

Bodil Gesslein, viktig del i gruppens backbone. Får saker att flyta. Hade med säkerhet varit en fenomenal kampanjchef för vilken kandidat som helst i nästa amerikanska presidentval.

Studenterna **Josefin Andersson**, **Cassandra Hennström**, **Rehan Chakari** och **Linn Engqvist** som alla gjort fina insatser i forskningsprojektet.

…

Poya Hård af Segerstad, person med oanade filosofiska talanger. Det har varit många och långa konversationer genom åren och för det mesta i en helt egen humoristisk genre. Lider av en stor brist: han är totalt oförmögen att ta in reglerna för hur en limerick ska vara uppbyggd.

Björn Stenström, ögonplastikkollega och rumskamrat. Han är ödmjuk, noggrann och en fantastisk kirurgisk pedagog för våra ST-läkare, vilket jag vet av egen erfarenhet.

Stellan Molander, med vem jag ofta hamnar i politiska diskussioner på hög nivå och humoristiska på låg dito. Jobbar hårt men försöker dölja det bakom en laid-back stil.

Andreas Machattos, munter och sympatisk kollega som ofta pratar rena grekiskan.

Anders Bergström, dåvarande verksamhetschef som vågade anställa mig för ett kort vikariat, trots att anställningsstoppen haglade som spön i backen och trots att jag var ett oprövat kort som inte ens genomfört min AT.

Våra vänner och kollegor i Stockholm, **Eva Dafgård Kopp** och **Elin Boman**, med vilka vi har ett givande och stimulerande samarbete.

…

Mina **vänner** från grundskolan, LTH-tiden och läkarprogrammet. Tack för alla roliga minnen och för framtida upplevelser.

Min svägerska **Eyllin** med familj. Du är som en syster för mig som genomgående visar stor entusiasm och ett genuint intresse för det som jag tar mig för i livet.

Mina svärföräldrar, **Anna** och **Julian**, som riskerade allt en gång i tiden för att ge sina barn en bättre framtid. Jag är så fantastiskt tacksam för det. Ni ställer alltid upp, för mig, för era barn och för era barnbarn.

Hela min stora och härliga **släkt** som skänkt mig så många fina minnen.

Mina mor- och farföräldrar, **Margareta, Ingemar, Signe** och **Allan** som alltid trott på mig och som varit de bästa förebilder.

Mina småbröder, **Staffan**, **Gustav** och **Erik** med respektive familjer. De flesta minnen från min barndom involverar minst en av er, och inte sällan er alla. Vi har spelat fotboll, strumpboll, snöboll och nintendoboll (?) ihop. Till en början räckte det med att vara störst och snabbast för att vinna över er men efterhand som de egenskaperna på något sätt överfördes från mig till er har jag fått utveckla andra färdigheter för att ha en chans.

Mina föräldrar, **Gabriella** och **Mats.** Tack för livet! Ni gav mig och mina syskon en fin och trygg uppväxt halvt ute på landet med djur, odlingar och oändliga lekytor. Ni körde oss fyra till ändlösa fotbollsträningar (helt förgäves skulle det visa sig) och har ställt upp i ur och skur.

Mina kära barn, **Vincent**, **Wilhelm** och **Eveline**. Ni är och kommer alltid att vara min största bedrift och det som jag är absolut mest stolt över. Det är en ynnest att få följa er utveckling från födsel till självständiga små individer med tilltagande viljestyrkor. Ni kan bli precis vad ni vill!

Min fru och livs kärlek, **Viviénne**. Jag kan inte föreställa mig vilka stordåd jag måste ha uträttat i tidigare liv för att förtjäna en person som du. Vi fann varandra redan under slutet av högstadiet och har varit oskiljaktiga sedan dess. Du är en fantastisk mamma och förebild för våra barn och det är sannolikt därför de har blivit så bra. Du är godhjärtad, intelligent, vacker och har ett skratt som gör att jag förälskar mig i dig gång på gång. Tack för allt!

References

1. Crouch, H.E., *History of basal cell carcinoma and its treatment.* J R Soc Med, 1983. **76**(4): p. 302-6.

2. Sontheimer, R.D., *Skin is not the largest organ.* J Invest Dermatol, 2014. **134**(2): p. 581-582.

3. Kechichian, E. and K. Ezzedine, *Vitamin D and the Skin: An Update for Dermatologists.* Am J Clin Dermatol, 2018. **19**(2): p. 223-235.

4. Arda, O., N. Goksugur, and Y. Tuzun, *Basic histological structure and functions of facial skin.* Clin Dermatol, 2014. **32**(1): p. 3-13.

5. Apalla, Z., et al., *Epidemiological trends in skin cancer.* Dermatol Pract Concept, 2017. **7**(2): p. 1-6.

6. Rastrelli, M., et al., *Melanoma: epidemiology, risk factors, pathogenesis, diagnosis and classification.* In Vivo, 2014. **28**(6): p. 1005-11.

7. Abbas, O., D.D. Miller, and J. Bhawan, *Cutaneous malignant melanoma: update on diagnostic and prognostic biomarkers.* Am J Dermatopathol, 2014. **36**(5): p. 363-79.

8. Rogers, H.W., et al., *Incidence Estimate of Nonmelanoma Skin Cancer (Keratinocyte Carcinomas) in the U.S. Population, 2012.* JAMA Dermatol, 2015. **151**(10): p. 1081-6.

9. Yu, M., et al., *Superficial, nodular, and morpheiform basal-cell carcinomas exhibit distinct gene expression profiles.* J Invest Dermatol, 2008. **128**(7): p. 1797-805.

10. Dourmishev, L.A., D. Rusinova, and I. Botev, *Clinical variants, stages, and management of basal cell carcinoma.* Indian Dermatol Online J, 2013. **4**(1): p. 12-7.

11. Angeles, C.V., S.L. Wong, and G. Karakousis, *The Landmark Series: Randomized Trials Examining Surgical Margins for Cutaneous Melanoma.* Ann Surg Oncol, 2019.

12. Nahhas, A.F., C.A. Scarbrough, and S. Trotter, *A Review of the Global Guidelines on Surgical Margins for Nonmelanoma Skin Cancers.* J Clin Aesthet Dermatol, 2017. **10**(4): p. 37-46.

13. Codazzi, D., et al., *Positive compared with negative margins in a single-centre retrospective study on 3957 consecutive excisions of basal cell carcinomas. Associated risk factors and preferred surgical management.* J Plast Surg Hand Surg, 2014. **48**(1): p. 38-43.

14. Beaulieu, D., et al., *Current perspectives on Mohs micrographic surgery for melanoma.* Clin Cosmet Investig Dermatol, 2018. **11**: p. 309-320.

15. Deinlein, T., et al., *The use of dermatoscopy in diagnosis and therapy of nonmelanocytic skin cancer.* J Dtsch Dermatol Ges, 2016. **14**(2): p. 144-51.

16.   Newlands, C., et al., *Non-melanoma skin cancer: United Kingdom National Multidisciplinary Guidelines.* J Laryngol Otol, 2016. **130**(S2): p. S125-S132.

17.   Walker, P. and D. Hill, *Surgical treatment of basal cell carcinomas using standard postoperative histological assessment.* Australas J Dermatol, 2006. **47**(1): p. 1-12.

18.   Kels, B.D., A. Grzybowski, and J.M. Grant-Kels, *Human ocular anatomy.* Clin Dermatol, 2015. **33**(2): p. 140-6.

19.   Slutsky, J.B. and E.C. Jones, *Periocular cutaneous malignancies: a review of the literature.* Dermatol Surg, 2012. **38**(4): p. 552-69.

20.   Collin, J.R.O., *A manual of systematic eyelid surgery*. 3rd ed ed. 2006, United Kingdom: Butterworth-Heinemann Elsevier.

21.   Errichetti, E. and G. Stinco, *Dermoscopy in General Dermatology: A Practical Overview.* Dermatol Ther (Heidelb), 2016. **6**(4): p. 471-507.

22.   Vestergaard, M.E., et al., *Dermoscopy compared with naked eye examination for the diagnosis of primary melanoma: a meta-analysis of studies performed in a clinical setting.* Br J Dermatol, 2008. **159**(3): p. 669-76.

23.   Sinz, C., et al., *Accuracy of dermatoscopy for the diagnosis of nonpigmented cancers of the skin.* J Am Acad Dermatol, 2017. **77**(6): p. 1100-1109.

24.   Cinotti, E., et al., *Dermoscopy for the diagnosis of eyelid margin tumours.* Br J Dermatol, 2019. **181**(2): p. 397-398.

25.   Xiong, Y.D., et al., *A meta-analysis of reflectance confocal microscopy for the diagnosis of malignant skin tumours.* J Eur Acad Dermatol Venereol, 2016. **30**(8): p. 1295-302.

26.   Cinotti, E., et al., *The role of in vivo confocal microscopy in the diagnosis of eyelid margin tumors: 47 cases.* J Am Acad Dermatol, 2014. **71**(5): p. 912-918.e2.

27.   Cinotti, E., et al., *Handheld In Vivo Reflectance Confocal Microscopy for the Diagnosis of Eyelid Margin and Conjunctival Tumors.* JAMA Ophthalmol, 2017. **135**(8): p. 845-851.

28.   Hernandez-Ibanez, C., et al., *Usefulness of High-Frequency Ultrasound in the Classification of Histologic Subtypes of Primary Basal Cell Carcinoma.* Actas Dermosifiliogr, 2017. **108**(1): p. 42-51.

29.   Dinnes, J., et al., *High-frequency ultrasound for diagnosing skin cancer in adults.* Cochrane Database Syst Rev, 2018. **12**: p. Cd013188.

30.   Pelosini, L., et al., *A novel imaging approach to periocular basal cell carcinoma: in vivo optical coherence tomography and histological correlates.* Eye (Lond), 2015. **29**(8): p. 1092-8.

31.   von Braunmuhl, T., et al., *Morphologic features of basal cell carcinoma using the en-face mode in frequency domain optical coherence tomography.* J Eur Acad Dermatol Venereol, 2016. **30**(11): p. 1919-1925.

32.   Pelosini, L., et al., *In vivo optical coherence tomography (OCT) in periocular basal cell carcinoma: correlations between in vivo OCT images and postoperative histology.* Br J Ophthalmol, 2013. **97**(7): p. 890-4.

33. Bydlon, T.M., et al., *Chromophore based analyses of steady-state diffuse reflectance spectroscopy: current status and perspectives for clinical adoption.* J Biophotonics, 2015. **8**(1-2): p. 9-24.

34. Garcia-Uribe, A., et al., *In vivo diagnosis of melanoma and nonmelanoma skin cancer using oblique incidence diffuse reflectance spectrometry.* Cancer Res, 2012. **72**(11): p. 2738-45.

35. Sheikh, R., et al., *Optimal Epinephrine Concentration and Time Delay to Minimize Perfusion in Eyelid Surgery: Measured by Laser-Based Methods and a Novel Form of Extended-Wavelength Diffuse Reflectance Spectroscopy.* Ophthal Plast Reconstr Surg, 2017.

36. Reistad, N., et al., *Diffuse reflectance spectroscopy of liver tissue.* SPIE Biophotonics South America. Vol. 9531. 2015: SPIE.

37. Dahlstrand, U., et al., *Identification of tumor margins using diffuse reflectance spectroscopy with an extended-wavelength spectrum in a porcine model.* Skin Res Technol, 2018. **24**(4): p. 667-671.

38. Nachabe, R., et al., *Estimation of biological chromophores using diffuse optical spectroscopy: benefit of extending the UV-VIS wavelength range to include 1000 to 1600 nm.* Biomed Opt Express, 2010. **1**(5): p. 1432-1442.

39. Reistad, N., et al. *Diffuse reflectance spectroscopy of liver tissue.* 2015.

40. Nilsson, J.H., et al., *Diffuse Reflectance Spectroscopy for Surface Measurement of Liver Pathology.* Eur Surg Res, 2017. **58**(1-2): p. 40-50.

41. Reistad, N., et al., *Intraoperative liver steatosis characterization using diffuse reflectance spectroscopy.* HPB (Oxford), 2019. **21**(2): p. 175-180.

42. Wang, L.V., *Prospects of photoacoustic tomography.* Med Phys, 2008. **35**(12): p. 5758-67.

43. Xu, D., et al., *Noninvasive and high-resolving photoacoustic dermoscopy of human skin.* Biomed Opt Express, 2016. **7**(6): p. 2095-102.

44. Luke, G.P., D. Yeager, and S.Y. Emelianov, *Biomedical applications of photoacoustic imaging with exogenous contrast agents.* Ann Biomed Eng, 2012. **40**(2): p. 422-37.

45. Attia, A.B.E., et al., *Noninvasive real-time characterization of non-melanoma skin cancers with handheld optoacoustic probes.* Photoacoustics, 2017. **7**: p. 20-26.

46. Breathnach, A., et al., *Preoperative measurement of cutaneous melanoma and nevi thickness with photoacoustic imaging.* J Med Imaging (Bellingham), 2018. **5**(1): p. 015004.

47. Breathnach, A., et al., *Assessment of cutaneous melanoma and pigmented skin lesions with photoacoustic imaging.* Photonic Therapeutics and Diagnostics Xi, 2015. **9303**.

48. Chuah, S.Y., et al., *Structural and functional 3D mapping of skin tumours with non-invasive multispectral optoacoustic tomography.* Skin Res Technol, 2017. **23**(2): p. 221-226.

49. Chuah, S.Y., et al., *Volumetric Multispectral Optoacoustic Tomography for 3-Dimensional Reconstruction of Skin Tumors: A Further Evaluation with Histopathologic Correlation.* J Invest Dermatol, 2018.

50. Favazza, C.P., et al., *In vivo photoacoustic microscopy of human cutaneous microvasculature and a nevus.* J Biomed Opt, 2011. **16**(1): p. 016015.

51. Grootendorst, D.J., et al., *First experiences of photoacoustic imaging for detection of melanoma metastases in resected human lymph nodes.* Lasers Surg Med, 2012. **44**(7): p. 541-9.

52. Kim, J., et al., *Multispectral ex vivo photoacoustic imaging of cutaneous melanoma for better selection of the excision margin.* Br J Dermatol, 2018. **179**(3): p. 780-782.

53. Valluru, K.S., K.E. Wilson, and J.K. Willmann, *Photoacoustic Imaging in Oncology: Translational Preclinical and Early Clinical Experience.* Radiology, 2016. **280**(2): p. 332-49.

54. Zhou, Y., et al., *Noninvasive Determination of Melanoma Depth using a Handheld Photoacoustic Probe.* J Invest Dermatol, 2017. **137**(6): p. 1370-1372.

55. Edwards, S.J., et al., *Diagnostic accuracy of reflectance confocal microscopy using VivaScope for detecting and monitoring skin lesions: a systematic review.* Clin Exp Dermatol, 2017. **42**(3): p. 266-275.

56. Toh, T.S., F. Dondelinger, and D. Wang, *Looking beyond the hype: Applied AI and machine learning in translational medicine.* EBioMedicine, 2019. **47**: p. 607-615.

57. Rajkomar, A., J. Dean, and I. Kohane, *Machine Learning in Medicine.* N Engl J Med, 2019. **380**(14): p. 1347-1358.

58. Wang, H. and G. Huang, *Application of support vector machine in cancer diagnosis.* Med Oncol, 2011. **28 Suppl 1**: p. S613-8.

59. Bae, Y., et al., *Automated network analysis to measure brain effective connectivity estimated from EEG data of patients with alcoholism.* Physiol Meas, 2017. **38**(5): p. 759-773.

60. Bak, N., et al., *Two subgroups of antipsychotic-naive, first-episode schizophrenia patients identified with a Gaussian mixture model on cognition and electrophysiology.* Transl Psychiatry, 2017. **7**(4): p. e1087.

61. Berikol, G.B., O. Yildiz, and I.T. Ozcan, *Diagnosis of Acute Coronary Syndrome with a Support Vector Machine.* J Med Syst, 2016. **40**(4): p. 84.

62. Sheikh, R., et al., *Clinical Translation of a Novel Photoacoustic Imaging System for Examining the Temporal Artery.* IEEE Trans Ultrason Ferroelectr Freq Control, 2019. **66**(3): p. 472-480.

63. Quickert, M. and A. Sorby, *The eyelids. Malposition of the lid.* Modern Ophthalmology, 1972. **2**: p. 937-954.

64. Bick, M.W., *Surgical management of orbital tarsal disparity.* Arch Ophthalmol, 1966. **75**(3): p. 386-9.

65. *Generic tissue optical properties.* 2019-12-15]; Available from: https://omlc.org/news/feb15/generic_optics/index.html.

66. Yudovsky, D. and L. Pilon, *Rapid and accurate estimation of blood saturation, melanin content, and epidermis thickness from spectral diffuse reflectance.* Appl Opt, 2010. **49**(10): p. 1707-19.

67. Cornejo, A., et al., *The use of visible light spectroscopy to measure tissue oxygenation in free flap reconstruction.* J Reconstr Microsurg, 2011. **27**(7): p. 397-402.

68. Volynskaya, Z., et al., *Diagnosing breast cancer using diffuse reflectance spectroscopy and intrinsic fluorescence spectroscopy.* J Biomed Opt, 2008. **13**(2): p. 024012.

69. Wilson, R.H., et al., *Review of short-wave infrared spectroscopy and imaging methods for biological tissue characterization.* J Biomed Opt, 2015. **20**(3): p. 030901.

70. Dieu, T. and A.M. Macleod, *Incomplete excision of basal cell carcinomas: a retrospective audit.* ANZ J Surg, 2002. **72**(3): p. 219-21.

71. Incel, P., M.S. Gurel, and A.V. Erdemir, *Vascular patterns of nonpigmented tumoral skin lesions: confocal perspectives.* Skin Res Technol, 2015. **21**(3): p. 333-9.

72. Vural, P., et al., *Lipid profile in actinic keratosis and basal cell carcinoma.* Int J Dermatol, 1999. **38**(6): p. 439-42.

73. Nijssen, A., et al., *Discriminating basal cell carcinoma from its surrounding tissue by Raman spectroscopy.* J Invest Dermatol, 2002. **119**(1): p. 64-9.

74. Kerkela, E. and U. Saarialho-Kere, *Matrix metalloproteinases in tumor progression: focus on basal and squamous cell skin cancer.* Exp Dermatol, 2003. **12**(2): p. 109-25.

75. Bunke, J., et al., *Extended-wavelength diffuse reflectance spectroscopy for a comprehensive view of blood perfusion and tissue response in human forearm skin.* Microvasc Res, 2019. **124**: p. 1-5.

76. Gloster, H.M., Jr. and K. Neal, *Skin cancer in skin of color.* J Am Acad Dermatol, 2006. **55**(5): p. 741-60; quiz 761-4.

77. Zeitouni, N.C., et al., *Preoperative Ultrasound and Photoacoustic Imaging of Nonmelanoma Skin Cancers.* Dermatologic Surgery, 2015. **41**(4): p. 525-528.

78. Stoffels, I., et al., *Metastatic status of sentinel lymph nodes in melanoma determined noninvasively with multispectral optoacoustic imaging.* Sci Transl Med, 2015. **7**(317): p. 317ra199.

79. Schwarz, M., et al., *Three-dimensional multispectral optoacoustic mesoscopy reveals melanin and blood oxygenation in human skin in vivo.* J Biophotonics, 2016. **9**(1-2): p. 55-60.

80. Yao, J. and L.V. Wang, *Photoacoustic Microscopy.* Laser Photon Rev, 2013. **7**(5).

81. Lin, L., et al., *In vivo photoacoustic tomography of myoglobin oxygen saturation.* J Biomed Opt, 2016. **21**(6): p. 61002.

82. Milz, S., et al., *An immunohistochemical study of the extracellular matrix of the tarsal plate in the upper eyelid in human beings.* J Anat, 2005. **206**(1): p. 37-45.